Pattern selection of solutions of the Swift-Hohenberg equation

Lambertus A. Peletier [1] **& Vivi Rottschäfer** [2]

Abstract. We study the large-time behaviour of solutions $u(x,t)$ of the Swift-Hohenberg equation on a one-dimensional domain $(0,L)$, focussing in particular on the role of the eigenvalue parameter α and the length L of the domain on the selection of the limiting profiles v. We show by means of numerical simulations how different values of these parameters may lead to qualitatively different final profiles, and prove the existence of a collection Σ_n of disjoint intervals, which depend on the value of α, such that if $L \in \Sigma_n$ then solutions all converge to the trivial solution $v = 0$. We show that branches of nontrivial solutions bifurcate from the trivial solution at the endpoints of these intervals and we study the local behaviour of these branches. We establish global bounds for the solutions $u(x,t)$ and identify the global attractor. Finally, we derive an estimate about the shape of the final state.

1 Introduction

In studies of pattern formation, the *Swift-Hohenberg equation*

$$\frac{\partial u}{\partial t} = \alpha\, u - \left(1 + \frac{\partial^2}{\partial x^2}\right)^2 u - u^3, \qquad \alpha \in \mathbf{R}, \tag{SH}$$

plays a central role. Proposed in 1987 by Swift & Hohenberg [21] in connection with Rayleigh-Bénard convection, it has since featured in a variety of problems, such as Taylor-Couette flow [14],[17], and in the study of lasers [15]. We also refer to the surveys given in [10] and [9] and the recent review [5].

The Swift-Hohenberg equation is interesting from the point of view of pattern formation, because it has many qualitatively different stable equilibrium solutions (cf. [4] and the survey given in [19]). This begs the question, which of these equilibrium solutions will be selected as time tends to infinity. In particular, we wish to know how this selection depends on parameters involved in the problem and on the choice of initial data.

To be more specific we study the Cauchy-Dirichlet problem for the Swift-Hohenberg equation (SH) on the interval $(0,L)$, where the length L is an important parameter. Thus,

[1] Mathematical Institute, Leiden University, PB 9512, 2300 RA Leiden & Centrum voor Wiskunde en Informatica, PB 94079, 1090 GB Amsterdam, The Netherlands; email: `peletier@math.leidenuniv.nl`

[2] Mathematical Institute, Leiden University, PB 9512, 2300 RA Leiden, The Netherlands; email: `vivi@math.leidenuniv.nl`

writing equation (SH) in a more conventional form, we consider the problem

$$\begin{cases} u_t = -u_{xxxx} - 2u_{xx} - f_\alpha(u) & \text{for} \quad 0 < x < L, \quad t > 0, & (1.1a) \\ u = 0 \quad \text{and} \quad u_{xx} = 0 & \text{at} \quad x = 0, L, \quad t > 0, & (1.1b) \\ u(x,0) = u_0(x) & \text{for} \quad 0 < x < L, & (1.1c) \end{cases}$$

where

$$f_\alpha(s) = (1-\alpha)s + s^3, \tag{1.2}$$

and u_0 is a smooth function that vanishes at $x = 0$ and $x = L$. In most of this article we will assume that u_0 is symmetric with respect to the center of the domain, i.e.

$$u_0(L - x) = u_0(x) \qquad \text{for} \qquad 0 < x < L. \tag{1.3}$$

Note that this assumption implies that the solution remains symmetric for all t.

Problem (1.1) is a *Gradient System* with corresponding *Lyapunov functional*

$$J(u; L) = \frac{1}{L}\int_0^L \left\{ \frac{1}{2}(u'')^2 - (u')^2 + F_\alpha(u) \right\} dx, \tag{1.4}$$

where

$$F_\alpha(u) = \int_0^u f_\alpha(s)\, ds = \frac{1-\alpha}{2}u^2 + \frac{1}{4}u^4. \tag{1.5}$$

This means (cf. [13]) that if the stationary solutions of Problem (1.1) are isolated, then $u(x,t)$ tends to one of these solutions as $t \to \infty$. Thus, in that case, for every $x \in (0, L)$:

$$u(x,t) \to v(x) \qquad \text{as} \qquad t \to \infty,$$

where $v(x)$ is a solution of the two-point boundary value problem

$$\begin{cases} v^{iv} + 2v'' + v^3 + (1-\alpha)v = 0 & \text{for} \quad 0 < x < L, \\ v = 0 \quad \text{and} \quad v'' = 0 & \text{at} \quad x = 0,\ L. \end{cases} \tag{1.6}$$

It is known that if $\alpha \leq 0$, then Problem (1.6) has the trivial solution only (cf. Chapter 9 of [19]), and hence, for every $x \in (0, L)$,

$$u(x,t) \to 0 \qquad \text{as} \qquad t \to \infty.$$

For $\alpha > 0$ the situation is much more complicated and, depending on the value of α and of L, there may be very many stationary profiles to choose from. In this article we make a start with answering the question, which of these profiles is chosen.

In order to gain insight into the different types of limiting behaviours and the effect of the parameter α and the length L of the domain on the final profile that is selected, we carried out a series of numerical simulations. In Figures 1 and 2 some of the results of these simulations are shown. Further results are presented in Section 2. In Figures 1 and 2 we have chosen $\alpha = 0.3$ and used the following initial function:

$$u_0(x) = A \sin\left(\frac{\pi x}{L}\right), \qquad A = \frac{1}{10}. \tag{1.7}$$

We find that for L sufficiently small, the solution vanishes as $t \to \infty$. However, we see in Figure 1 that for larger values of L, the solution evolves into different periodic patterns as $t \to \infty$: for $L = 3$ the final profile v is qualitatively similar to that of the initial profile and half a period of a sine-like profile fills the entire domain $(0, L)$. Then, for $L = 6$ something surprising happens: the final profile is again the trivial solution $v = 0$, as it is for L small. When L is increased to $L = 9$ the final profile is nontrivial again. However, now it is a periodic profile that packs *three* half periods into $(0, L)$.

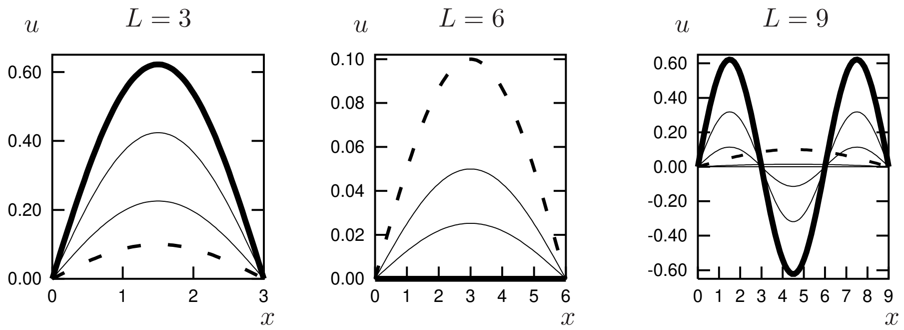

Figure 1: Profiles for $\alpha = 0.3$ and different choices of L : 3, 6 and 9. The dashed curve is the initial profile (1.7) and the thick curve the final profile. The other curves represent profiles at intermediate times.

In Figure 2 we show how the L^2-norm of the final profile v, scaled to take into account the length of the domain,

$$\|v\|^2 = \frac{1}{L} \int_0^L v^2(x)\, dx, \tag{1.8}$$

varies with respect to L. We see that there exist critical values L_1 and L_2 of L, such that for $L \le L_1$ and $L_2 \le L \le 3L_1$ the final profile v is identically zero, whilst for $L \in (L_1, L_2)$ and for larger values of L it is not. The dotted lines correspond to values of L for which the solution graphs are shown in Figure 1.

We will prove that there exist critical lengths, $L_1(\alpha)$ and $L_2(\alpha)$, given by

$$L_1(\alpha) = \frac{\pi}{\sqrt{1+\sqrt{\alpha}}} \qquad \text{and} \qquad L_2(\alpha) = \frac{\pi}{\sqrt{1-\sqrt{\alpha}}}, \qquad 0 < \alpha < 1, \tag{1.9}$$

where branches of nontrivial solutions of Problem (1.6) bifurcate from the trivial solution.

Remark. Note that $L_2(\alpha)$ is only defined for $\alpha \in (0, 1)$. In this article we focus on values of α in this range. However, in Section 2 we report on a few numerical simulations carried out for $\alpha = 1.25$ and $\alpha = 2$. For $\alpha > 1$ the potential function F_α defined in (1.5) is a *double well* potential, with local minima at $u = \pm\sqrt{\alpha - 1}$, and if $\alpha = 2$ we see a qualitatively different final state. This will be the subject of future research.

The precise behaviour of the solution branches near the points $(L_1, 0)$ and $(L_2, 0)$ in the (L, v)-plane is given in the following theorem.

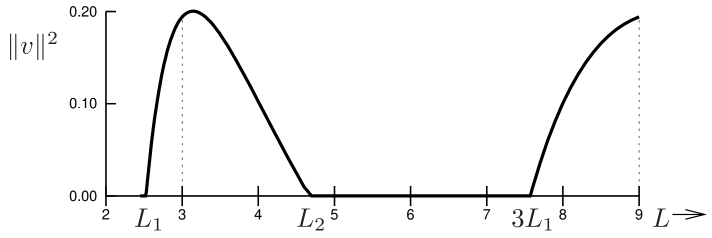

Figure 2: Graph of the L^2-norm of the final profile for $\alpha = 0.3$ and $L \in [2, 9]$.

Theorem 1.1 *Let $0 < \alpha < 1$. At each of the points $(L_1, 0)$ and $(L_2, 0)$ in the (L, v)-plane, a branch of nontrivial solutions of Problem (1.6) bifurcates from the trivial solution. The local behaviour of these branches is given by*

$$\|v\|^2 \sim \frac{3}{8\pi}\sqrt{\alpha}\,(1+\sqrt{\alpha})^{3/2}(L - L_1) \qquad as \qquad L \searrow L_1,$$
$$\|v\|^2 \sim \frac{3}{8\pi}\sqrt{\alpha}\,(1-\sqrt{\alpha})^{3/2}(L_2 - L) \qquad as \qquad L \nearrow L_2.$$

In addition, we prove that when α is such that $L_2(\alpha) < 3L_1(\alpha)$, which is the case when $0 < \alpha < \frac{16}{25}$, and L is chosen in the interval $[L_2, 3L_1]$, then

$$u(t) \to 0 \qquad \text{as} \qquad t \to \infty. \tag{1.10}$$

This confirms what was observed in the simulations depicted in Figures 1 and 2.

Remark. We will refer to the intervals, such as $[L_2, 3L_1]$ in Figure 2, where the solution converges to the trivial solution, as *Gaps*.

In a similar manner, there exist two or more gaps if $3L_2(\alpha) < 5L_1(\alpha)$. This is the case when $0 < \alpha < \frac{64}{289}$.

More generally, a simple computation shows that

$$(2n-1)L_2 < (2n+1)L_1 \qquad \text{if} \qquad \alpha < \alpha_n \stackrel{\text{def}}{=} 4\{2n + (2n)^{-1}\}^{-2}, \qquad n = 1, 2, \ldots.$$

In the following theorem we state the existence of at least n gaps for values of L in the set

$$\Sigma_n \stackrel{\text{def}}{=} (0, L_1] \cup [L_2, 3L_1] \cup \cdots \cup [(2n-1)L_2, (2n+1)L_1]. \tag{1.11}$$

Theorem 1.2 *Let $u(t)$ be the solution of Problem (1.1) in which $\alpha < \alpha_n$ for some $n \geq 1$. Then, for all $L \in \Sigma_n$,*

$$u(t) \to 0 \qquad as \qquad t \to \infty.$$

These results can be understood by studying the linear stability of the trivial solution. We are led to the eigenvalue problem obtained from Problem (1.1) by substituting $u(x,t) = e^{-\lambda t}\varphi(x)$ and omitting the nonlinear term:

$$\begin{cases} \varphi^{iv} + 2\varphi'' + (1-\alpha)\varphi = \lambda\varphi & \text{for} \quad x \in (0, L), \\ \varphi = 0 \quad \text{and} \quad \varphi'' = 0 & \text{at} \quad x = 0,\ L. \end{cases} \tag{1.12}$$

The eigenfunctions and the eigenvalues of Problem (1.12) are given by

$$\varphi_n(x) = \sqrt{2}\,\sin\Big(\frac{n\pi x}{L}\Big) \qquad \text{and} \qquad \lambda_n = \lambda_n(L) = P\Big(\frac{n\pi}{L}\Big), \tag{1.13}$$

where $P(\xi)$ is the symbol of the left hand side of the differential equation in (1.12):

$$P(\xi) = (\xi^2 - 1)^2 - \alpha. \tag{1.14}$$

The eigenfunctions are orthonormal, and have been normalised so that $\|\varphi_n\| = 1$. In Figure 3 we give graphs of $P(\xi)$ and $P(n\pi/L)$ for $n = 1, 2, 3$. The critical lengths L_1 and L_2 correspond to the zeros of λ_1, i.e. of $P(\pi/L)$. Thus, $L_1 = \pi/\xi_+$ and $L_2 = \pi/\xi_-$, where $P(\xi_\pm) = 0$. The zeros of λ_n are nL_1 and nL_2.

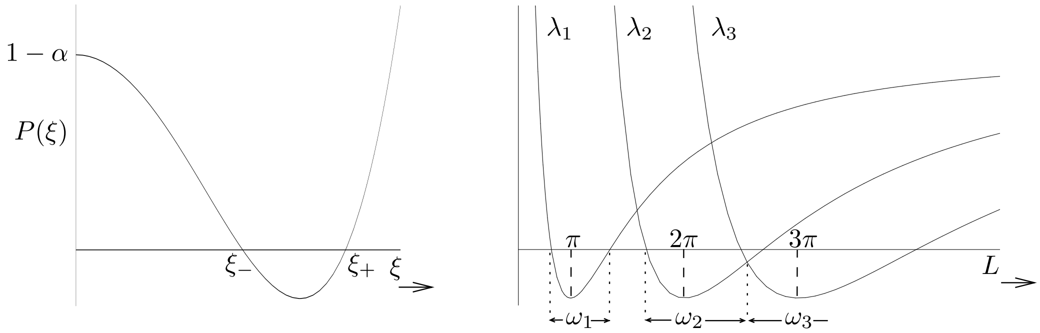

Figure 3: Graphs of the polynomial $P(\xi)$ and of the eigenvalues $\lambda_n = P(n\pi/L)$ as a function of L for $n = 1, 2$ and 3.

The linear stability of the trivial solution with respect to symmetric perturbations depends on the smallest eigenvalue:

$$\mu(L) = \inf\{\lambda_n(L) : n \geq 1,\ n \text{ odd}\}. \tag{1.15}$$

One finds that if $\alpha \leq \alpha_n$, then $\mu(L) \geq 0$ for $L \in \Sigma_n$, and $u = 0$ is linearly stable for symmetric perturbations. Using energy estimates we show that this implies that $u = 0$ is a global attractor.

As soon as one of the eigenvalues becomes negative, then $\mu(L) < 0$ and the trivial solution is linearly unstable for symmetric perturbations. For such values of L we show that the solution $u(t)$ has the following property:

$$\limsup_{t\to\infty} \|u(t)\| \leq \sqrt{|\mu|},$$

i.e. the ball $B(0, R)$, with $R = \sqrt{|\mu|}$, is a *Global Attractor*.

In order to identify the final profile for different values of L it will be convenient to introduce the intervals ω_n in which $\mu = \lambda_n$ and $\mu < 0$, $n = 1, 2, \ldots$, i.e. the intervals in which λ_n is the smallest eigenvalue and also negative (see Figure 3). For every $n \geq 1$, the interval ω_n contains the length $L = n\pi$. Note that $\omega_1 = (L_1, L_2)$ if $\alpha \in (0, \frac{16}{25})$.

Problem (1.1) being a gradient system, the solution $u(t)$ often converges to a global minimiser of the problem

$$\Phi(L) = \min\{J(u; L) : u \in X\}, \tag{1.16}$$

where $X = H^2(0, L) \cap H_0^1(0, L)$. The existence of such a minimiser is well known for any $L > 0$ and $\alpha \in \mathbf{R}$ [7],[20],[22]. Here, we make the additional assumption that X contains the *symmetric* functions only, i.e. we assume that functions $w \in X$ are endowed with the symmetry property $w(L - x) = w(x)$.

We prove the following bounds for $J(u)$ and $\|u\|$:

Theorem 1.3 *Suppose that u is a global minimiser of Problem (1.16), and that $\alpha \in (0, 1)$. Then,*

$$\begin{aligned} J(u; L) &\leq -\frac{1}{6}\left|P\left(\frac{\pi}{L}\right)\right|^2 \qquad \text{for} \qquad L \in (L_1, L_2), \\ J(u; L) &\geq -\frac{1}{4}\left|P\left(\frac{\pi}{L}\right)\right|^2 \qquad \text{for} \qquad L \in \omega_1, \end{aligned} \tag{1.17}$$

and

$$\left(1 - \frac{1}{\sqrt{3}}\right)\left|P\left(\frac{\pi}{L}\right)\right| \leq \|u\|^2 \leq \left(1 + \frac{1}{\sqrt{3}}\right)\left|P\left(\frac{\pi}{L}\right)\right| \qquad \text{for} \qquad L \in \omega_1. \tag{1.18}$$

In Figure 4, we show the graph of $J(v; L)$ versus L for the final profile v, obtained in the numerical simulations with $\alpha = 0.3$ and u_0 given by (1.7). Although we do not know that this numerically obtained function v is a global minimiser of (1.16), we conjecture that in this case it is.

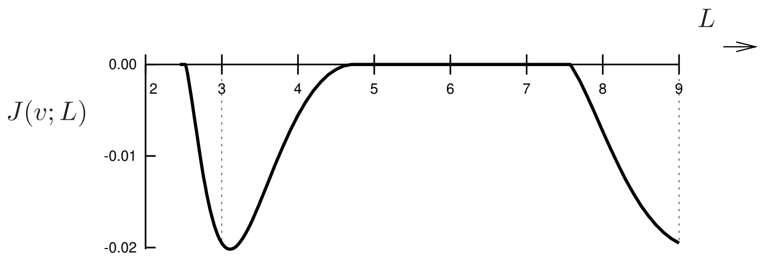

Figure 4: Graph of the action $J(v; L)$ of the final profile v for $\alpha = 0.3$ and $L \in [2, 9]$.

An important quantity associated with stationary solutions of the Swift-Hohenberg equation, i.e. with solutions v of Problem (1.6), is the *Energy* $\mathcal{E}(v; L)$ defined by

$$\mathcal{E}(v; L) = v'v''' - \frac{1}{2}(v'')^2 + (v')^2 + F_\alpha(v). \tag{1.19}$$

It is the first integral of the ordinary differential equation for v given in (1.6), and thus it is constant over the interval $(0, L)$. In Figure 5, we give the graph of $\mathcal{E}(v; L)$ for the final state v when $\alpha = 0.3$.

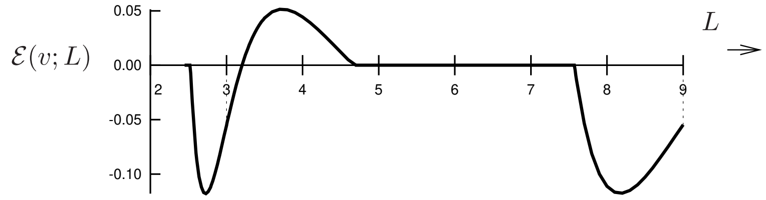

Figure 5: Graph of the energy $\mathcal{E}(v; L)$ of the final profile v for $\alpha = 0.3$ and $L \in [2, 9]$.

In Section 7 we show that if the function $\Phi(L) = \inf J(\cdot; L)$ has a local minimum at, say $\overline{L}$ and a solution $\overline{v}$, then $\Phi(\overline{L}) = J(\overline{v}; \overline{L}) = \mathcal{E}(\overline{v}; \overline{L})$. This property is nicely borne out by the numerical simulations shown in Figures 4 and 5, as well as in those shown in Section 2.

Our final result concerns the *Shape* of the minimiser. Numerical results reveal a remarkable resemblance of minimisers, even those with a fairly large amplitude, to an appropriate multiple of the eigenfunction φ_1 when $L \in \omega_1$. The following result shows that this is no mere coincidence. Assuming that u is a minimiser of Problem (1.16), we write it as

$$u = a_1\varphi_1 + w, \qquad a_1 = (u, \varphi_1). \tag{1.20}$$

Then w lies in the orthogonal complement of the ray $\mathcal{S}_1 = \{t\varphi_1 : t \in \mathbf{R}\}$ spanned by φ_1. The quotient $\|w\|/a_1$ is the tangent of the angle θ between u and φ_1 and so it is a measure for the distance between u and $\mathcal{S}_1$. For this quantity we find the following bound:

$$\tan^2\theta = \frac{\|w\|^2}{a_1^2} \le \frac{1}{4}\sqrt{3}\,(\sqrt{3}+1)\,\frac{\left|P\left(\frac{\pi}{L}\right)\right|}{P\left(\frac{3\pi}{L}\right)} \qquad \text{for} \qquad L \in \omega_1 \cap (L_1, 3L_1]. \tag{1.21}$$

For minimisers – even the larger ones – we find that θ is still very small. For instance, suppose that $\alpha = 0.3$ and $L = \pi$, so that the global minimiser u of $J(u; L)$ is quite large (compare with Figure 1a, where $L = 3$). Then the above bound shows that $\theta \le 0.0745\ldots$. Hence u is still very close to $\mathcal{S}_1$, implying that it is close to an appropriate multiple of φ_1.

The organisation of this paper is the following. In Section 2, we present results of a series of numerical simulations for $\alpha = 0.3$, 0.5 and 0.9 and few for $\alpha = 1.25$ and $\alpha = 2$. After a some preliminaries in Section 3 which include notation and two calculus inequalities, we analyse in Section 4 the linear eigenvalue problem (1.12). In Section 5, we carry out the bifurcation analysis at the critical lengths L_1 and L_2. Then, in Section 6, we derive a several global bounds for solutions of Problem (1.1), which yield as a corollary the convergence of solutions of the full nonlinear problem to the trivial solution on certain ranges of L (see Theorem 1.2). Finally, in Section 7 we derive estimates about the size and shape of global minimisers of Problem (1.16).

A preliminary announcement of these results appeared in [18].

Acknowledgement. The authors are grateful to Santiago Betelu, Laurent Dimenza and Jan Just Keijser for assisting with the numerical computations.

2 Numerical simulations

In this section we present results of numerical simulations carried out in order to investigate how the final state $v(x)$ depends on the length of the interval L and the eigenvalue parameter α. We fix an appropriate initial function

$$u(x,0) = A\sin\left(\frac{\pi x}{L}\right) \qquad \text{for} \qquad 0 \le x \le L, \qquad A = \frac{1}{10},$$

and follow the solution $u(x,t)$ of Problem (1.1) numerically as $t \to \infty$ for different values of L and α. Since this initial function is symmetric with respect to $x = \frac{1}{2}L$, the solution $u(x,t)$ will be endowed with this same symmetry property for every $t > 0$ and the final state $v(x)$ will have this property too. Therefore,

$$v(x) = v(L-x) \qquad \text{for} \qquad 0 \le x \le L.$$

We first give results of simulations for three different values of α: 0.3, 0.5 and 0.9, and for each of these we vary the length L continuously from $L = 2.5$ to $L = 15$. The results of these three runs are given in the three families of figures below.

Case 1: $\alpha = \mathbf{0.3}$.
We find that for L small enough, for example when $L = 2.5$, the solution tends to the trivial solution, as seen in Figure 6 a. Here, by small enough we mean $L < L_1$, where the length L_1 has been introduced in the Introduction. However, for $L = 3$ this is no longer true and the trivial solution appears to be unstable, see Figure 6 b. This phenomenon is familiar; it is also found in the Dirichlet problem of second order equations, such as the Allen-Cahn equation, or the Fisher-Kolmogorov equation, where a stable solution bifurcates from the trivial solution at some critical value of L. We find that for $L = 3$ the limiting solution has one sign, as is the case in such second order equations. However, as we increase L further, something very surprising happens: beyond some critical value of L, once again, the solution tends to the trivial solution, as shown for $L = 6$ in Figure 6 c. This state of affairs continues to be true as we increase L. However, at $L = 9$ we find that the final state is nontrivial again; now it does change sign on the interval $(0, L)$; see Figure 6 d.

Case 2: $\alpha = \mathbf{0.5}$.
For this choice of α the results, shown in Figure 7, are qualitatively the same as those for $\alpha = 0.3$, except that since we increase L further, we encounter three qualitatively different nontrivial final states. For $L = 4.0$ the solution converges to a nontrivial state with no zeros on $(0, L)$, for $L = 6.0$ the final state is the trivial solution and for $L = 7.3$ the final state is nontrivial again, but with two zeros on $(0, L)$. Finally, for $L = 14$ the final state is also nontrivial, but now it has four zeros.

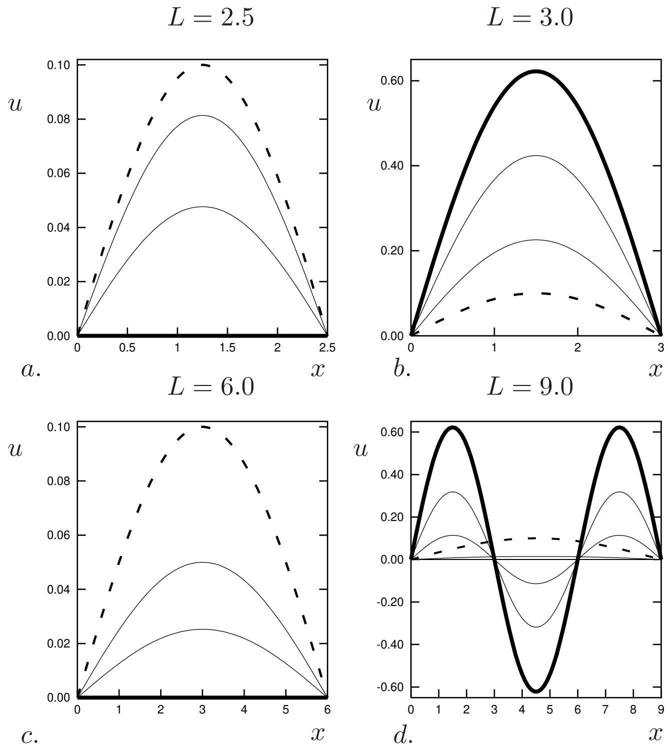

Figure 6: Evolution of solution profiles for $\alpha = 0.3$ and $L = 2.5,\ 3.0,\ 6.0$ and $L = 9.0$. The dashed curve is the initial profile and the thick curve is the final profile. The other curves represent profiles at intermediate times.

Case 3: $\alpha = \mathbf{0.9}$.

For this choice of α we no longer find any value of $L > L_1$ for which the solution converges to the trivial solution. As in the previous cases the final state $v(x)$ passes through several qualitatively different shapes as we increase L: for $L = 4.0$ and $L = 6.0$ the function $v(x)$ has one sign and is concave on $(0, L)$ (see Figures. 8 a. and 8 b.). However, at $L = 6.0$ the top of v has flattened. For $L = 7.0$ and $L = 7.2$ (see Figures. 8 c. and 8 d.) v still has one sign, but it is no longer concave: a *dimple* has developed which becomes more pronounced as L increases. Then, when L is chosen just a little larger – $L = 7.3$ – the final profile has a completely different shape: the dimple has grown so large that $v(x)$ has *two* zeros (see Figure 8 e.). Increasing L further, to $L = 14.0$, the final profile jumps to a solution with *four* zeros (see Figure 8 f.), similar to the one observed in the previous case.

In the Figures 6, 7 and 8 we gave the results of numerical simulations for only a few isolated values of L. To complete the picture we show in Figure 9 how for $\alpha = 0.3,\ 0.5$ and

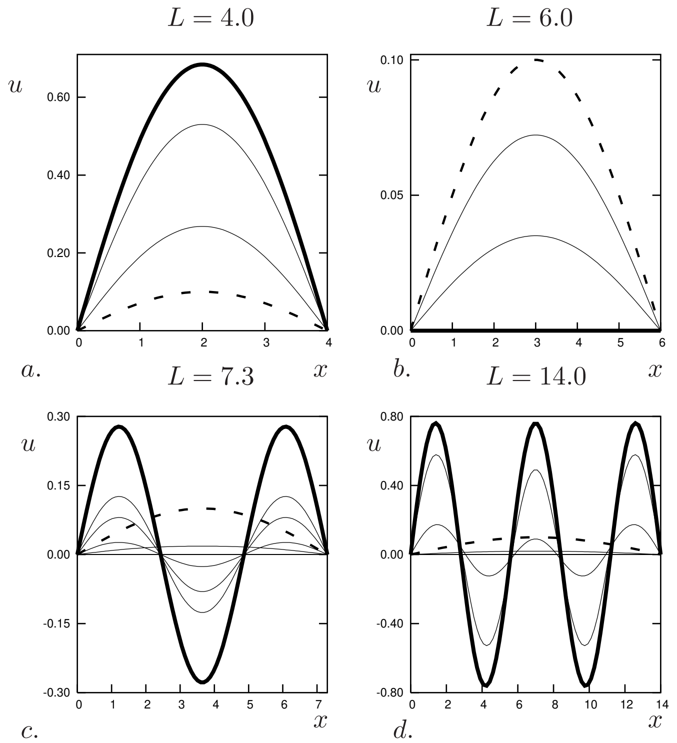

Figure 7: Evolution of profiles for $\alpha = 0.5$ and $L = 4.0,\ 6.0,\ 7.3$ and $L = 14.0$. The dashed curve is the initial profile and the thick curve the final profile. The other curves represent profiles at intermediate times.

0.9, the scaled L^2-norm $\|v\|$ of the final profile $v(x)$ changes as L increases. We recall that

$$\|v\|^2 = \frac{1}{L}\int_0^L v^2(x)\,dx.$$

The graphs in Figure 9 elucidate the phenomena we observed in Figures 6, 7 and 8. For $\alpha = 0.3$ we now see how a branch of final solutions $v(x)$ bifurcates off the trivial solution at $L = L_1$ and returns again at $L = L_2$ where L_1 and L_2 were defined in (1.9). As L is increased further, we see that a new branch bifurcates at $L = 3L_1$. This branch extends to $L^* \approx 13$, where we find a discontinuity. For values of L in the interval (L_1, L_2), the function v has one sign, whilst for $L > 3L_1$ it is more complex. It has acquired *two* zeros on $(0, L)$ for $3L_1 < L < L^*$ and *four* zeros just beyond L^*.

For $\alpha = 0.5$ we obtain an analogous picture. However, we see that the first interval (or 'gap') $[L_2, 3L_1]$, in which the final state is $v = 0$, has become smaller. The second

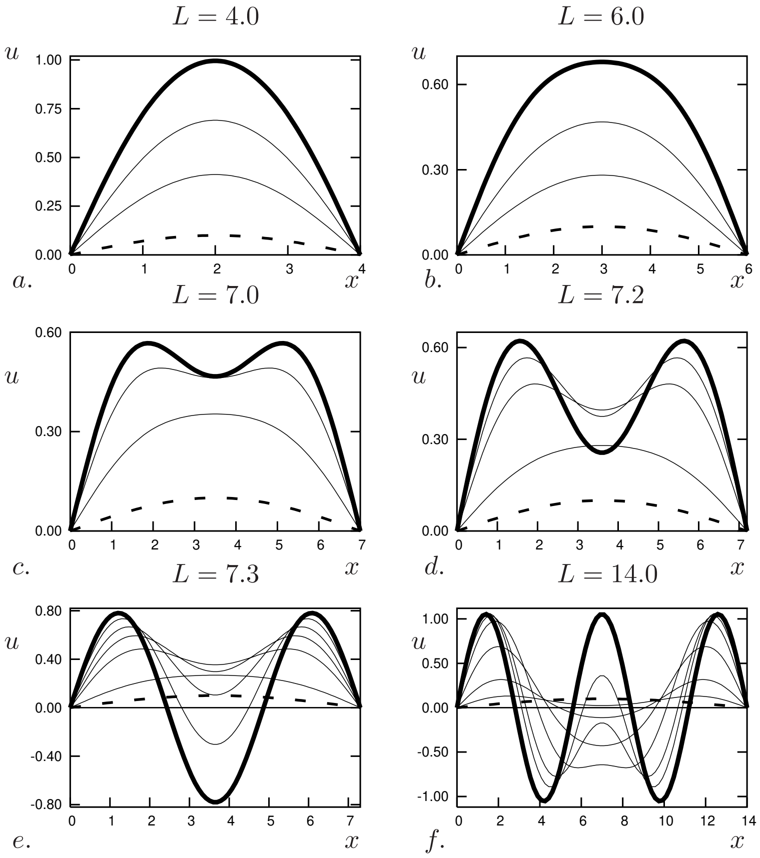

Figure 8: Evolution of solution profiles for $\alpha = 0.9$ and $L = 4.0,\ 6.0,\ 7.0,\ 7.2,\ 7.3$ and $L = 14.0$. The dashed curve is the initial profile and the thick curve the final profile. The other curves represent profiles at intermediate times.

branch, which bifurcates at $3L_1$ now extends to a value $L^* \approx 13.4$, where we again find a discontinuity: for L just *below* L^*, v has *two* zeros, whilst for L just *above* L^* it has *four* zeros on $(0, L)$.

For $\alpha = 0.9$ we find that there no longer is a gap, i.e. for every $L \in (2.5, 14)$ the final profile is nontrivial. The graph of $\|v\|$ has two discontinuities, one at $L^* \approx 7.2$: where the final state v changes from a solution without zeros to one with two zeros, and a discontinuity at $L^{**} \approx 13.9$, where v changes from a solution with two zeros to one with four zeros.

In the table below we give the values of L_1 and L_2, as determined by using the analytical

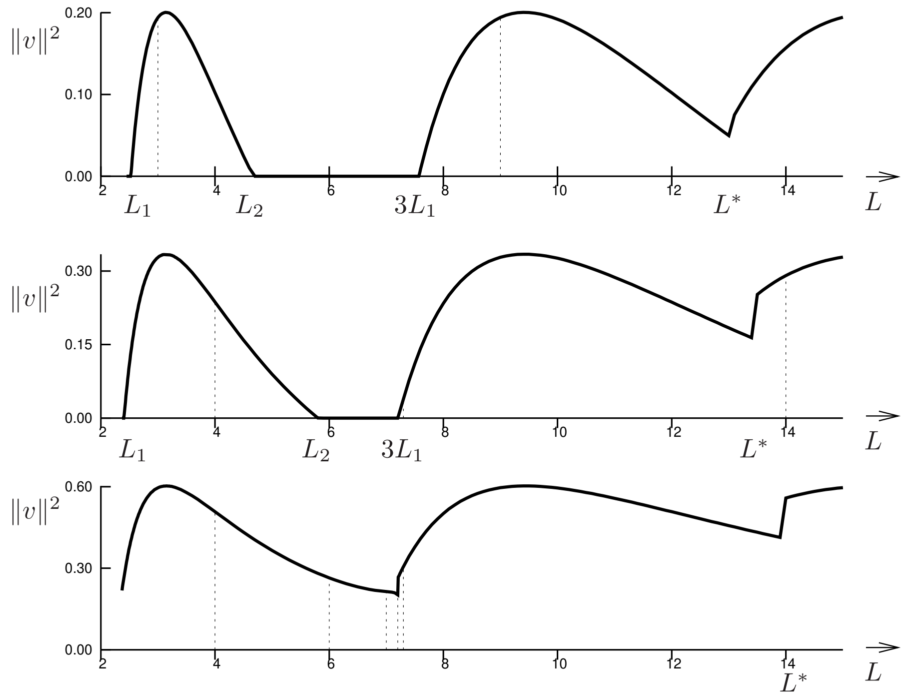

Figure 9: Graphs of the L^2-norm of the final profile for $\alpha = 0.3$ (top), 0.5 and 0, 9 (bottom), as L varies.

expressions (1.9), for the three values of α, as well as the ordering of L_2 and $3L_1$: if $L_2 < 3L_1$ there exists a gap.

α	L_1	L_2	$3L_1$	*gaps*
0.3	2.525	4.67	7.58	for $L_2 < 3L_1$
0.5	2.40	5.80	7.21	for $L_2 < 3L_1$
0.9	2.25	13.87	6.75	no gaps ($L_2 > 3L_1$)

Table 1: The values of L_1, L_2 and $3L_1$ computed analytically in Section 4 for $\alpha = 0.3,\ 0.5$ and $\alpha = 0.9$. Included is also the range of L-values where a gap exists.

The numerical results of Figure 9 and the analytical ones in Table 1 are found to compare very well.

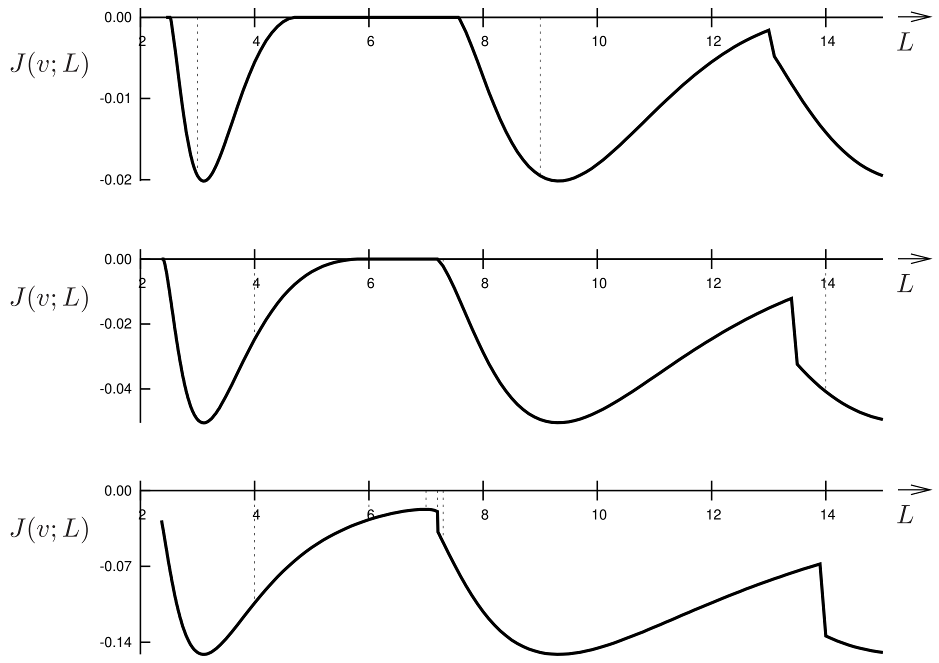

Figure 10: Graph of the action $J(v; L)$ of the final profile for $\alpha = 0.3$ (top), 0.5 and 0.9 (bottom)

In Figure 10 we plot the action $J(v; L)$ for different values of α. Obviously, the gap behaviour is also apparent here. We see that the gaps become smaller as α increases. We also note that the local minima have the same value. Note that whereas the branch of $\|v\|^2$ makes a nonzero angle with the axis at L_1 and L_2, the branch of $J(v; L)$ is tangent to the axis at L_1 and L_2. This is consistent with the local analysis given in Section 5.

In Figure 11 we plot the energy $\mathcal{E}(v; L)$ of the final state v. Note that between L_1 and L_2 the branch crosses the axis. This means that there exist periodic solutions with zero energy for some $L \in (L_1, L_2)$. Comparing Figures 10 and 11, we also note that at the local minima of J we have $J = \mathcal{E}$. This observation is proved in Section 7.

From these numerical simulations, an interesting observation can be made about the *Shape* of the final profile. It was found that when $\alpha = 0.3$ and $L \in (L_1, L_2)$ the graph of $v(x)$ looks strikingly similar to an appropriate multiple of the first eigenfunction $\varphi_1(x)$ of the eigenvalue problem (1.12) obtained by linearising about the trivial solution. This continues

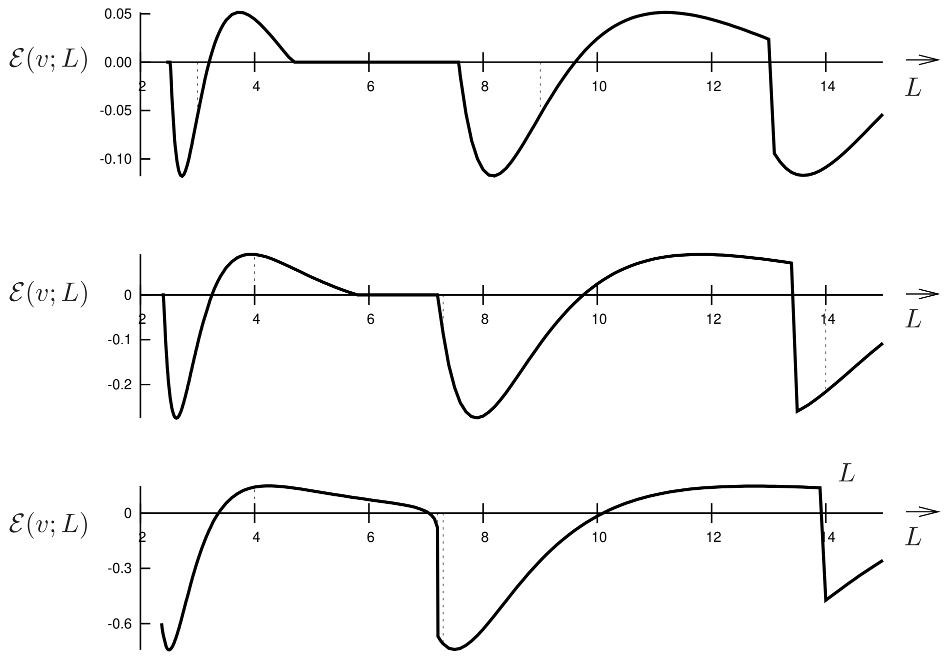

Figure 11: Graph of the energy $\mathcal{E}(v;L)$ of the final profile for $\alpha = 0.3$ (top), 0.5 and 0.9 (bottom)

to be true even when v is not particularly small and lies in a region where nonlinear effects would be expected to come into play. Analogous similarities were found for larger values of L, when the final state has two or more zeros. In Section 7 we will see that this phenomenon is closely related to the fact that this is a *fourth* order problem, and we conjecture that a similar phenomenon – and then even stronger – will arise in *sixth* order equations (cf. [8]).

The simulations presented so far have all been done for values of $\alpha \in (0,1)$. The potential $F_\alpha(s)$ then has a single well, which is located at the origin. Below we include two simulations for values of $\alpha > 1$. In that case, $F_\alpha(s)$ has two wells, located at $s = \pm\sqrt{\alpha - 1}$. In Figure 12 we take $\alpha = 2$. We see that for larger values of L solutions appear to converge to the center of one of the wells: $+\sqrt{\alpha-1}$. We conjecture that as L becomes very large, the solution $u(x,t)$ will converge to a profile v which is composed of two half-kinks: on any bounded set $[0, A]$, where A is some positive constant, the solution tends to a heteroclinic orbit which is odd with respect to the origin, and tends to $\pm\sqrt{\alpha-1}$ as $x \to \pm\infty$. Similarly,

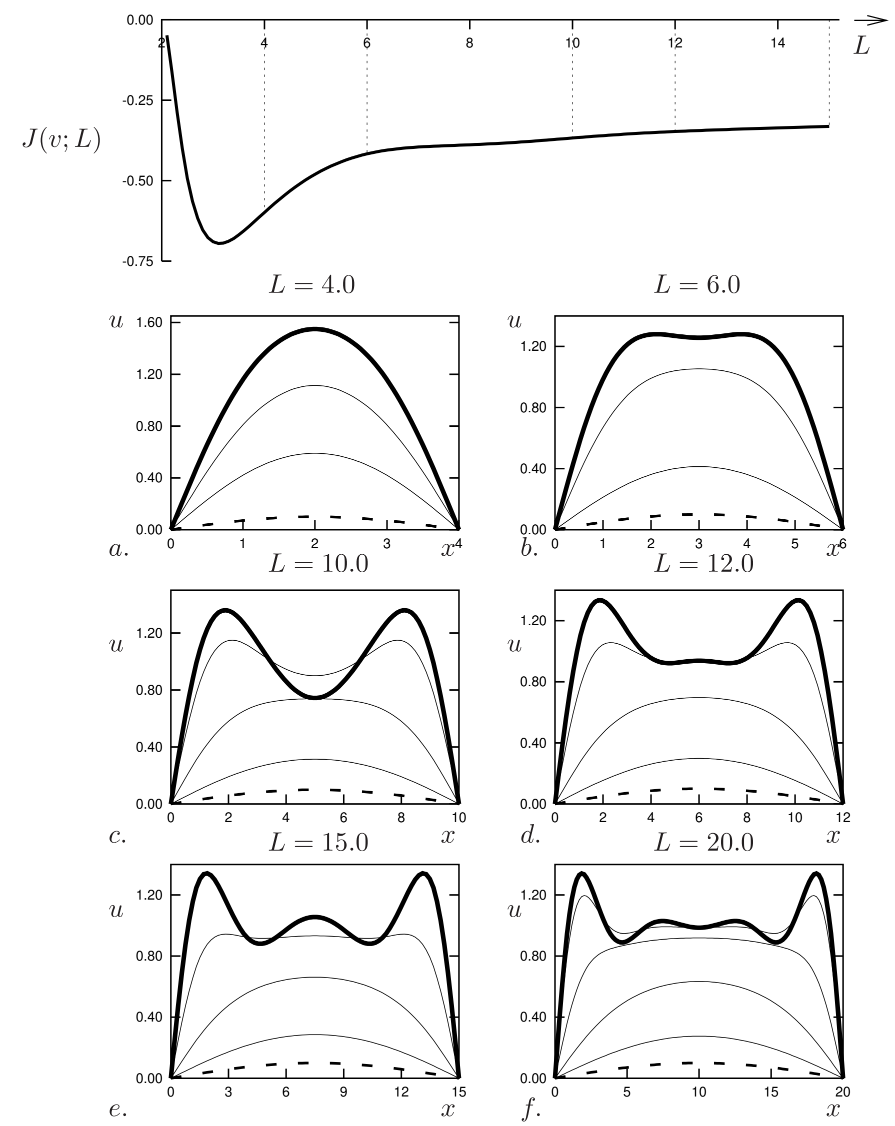

Figure 12: The action J and solution profiles for $\alpha = 2.0$ and $L = 4.0,\ 6.0,\ 10.0,\ 12.0,\ 15.0$ and $L = 20.0$. The dashed curve is the initial profile and the thick curve the final profile. The other curves represent profiles at intermediate times.

on any bounded interval $[L - A, L]$ the solution tends to a heteroclinic orbit which is odd with respect to $x = L$ and tends to $\mp\sqrt{\alpha - 1}$ as $x \to \pm\infty$. We also note that $J(v; L)$

appears to converge to $-\frac{1}{4}$ as $L \to \infty$ which is consistent with the above observation, since $J(\sqrt{\alpha - 1}; L) = -\frac{1}{4}(\alpha - 1)^2 = -\frac{1}{4}$ for $\alpha = 2$.

Numerical evidence (cf. [19], Figure 1.3.3) suggests that such heteroclinic orbits only exist if $\alpha \geq \alpha^* = 1.6983\ldots$, raising the question as to what happens for large time when $1 < \alpha < \alpha^*$. Motivated by this question, we carried out a numerical simulation for $\alpha = 1.25$ (see Figure 13). We see that the final profile is now quite different from what was observed for $\alpha = 2$. This transition will be addressed in a forthcoming study.

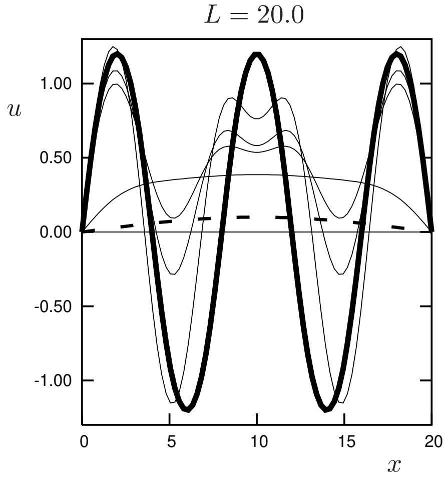

Figure 13: Evolution of profiles for $\alpha = 1.25$ and $L = 20.0$. The dashed curve is the initial profile and the thick curve the final profile. The other curves represent profiles at intermediate times.

We conclude with a few remarks about the method we used to obtain the above numerical results. For the simulations, we designed a FORTRAN-programme that iterated Problem (1.1) forward in time. To find stationary solutions we introduced a stop-condition that terminates the simulation when for several time steps no significant change was observed. The second and fourth derivative that occur in the equation are introduced by using the method of central difference, i.e. the first and the second derivative were defined by

$$u_x(x_i) = \frac{u(x_{i+1}) - u(x_{i-1})}{x_{i+1} - x_{i-1}} \quad \text{and} \quad u_{xx}(x_i) = \frac{u(x_{i+2}) - 2u(x_i) + u(x_{i-2})}{(x_{i+1} - x_{i-1})2},$$

and the fourth order derivative was represented in a similar fashion. The grid points x_i were chosen equidistant. For most of the simulations we have taken 80 grid points in the interval $[0, L]$, although for small values of L we decreased the number of grid points, whereas for larger values of L we increased it.

We noticed that the numerical simulations were extremely sensitive to the way the initial condition was defined. To ensure that $u(x, 0)$ is symmetric, and that $u(x, t)$ remains symmetric for all time, we define the initial condition on $[0, \frac{1}{2}L]$ by putting

$$u(x,0) = A\sin\Big(\frac{\pi x}{L}\Big) \qquad \text{for} \qquad 0 \le x \le \frac{1}{2}L,$$

and then reflected this function with respect to $x = \frac{1}{2}L$ in order to define $u(x, 0)$ on $[\frac{1}{2}L, L]$. By using this construction, the initial condition is symmetric with respect to $x = \frac{1}{2}L$ up to every decimal place, and we found in the simulations that the solution remains symmetric for all time.

3 Preliminaries

In this section we introduce some notation, define the notion of a solution and derive two basic calculus inequalities.

Let $Q = \{(x,t) : 0 < x < 1,\ t > 0\}$. By a solution of Problem (1.1) we mean a function $u(x,t)$ defined on $\overline{Q}$ endowed with the following properties:
(i) $u \in C^{4,1}(Q) \cup C(\overline{Q})$,
(ii) u_{xx} is continuous up to the lateral boundary $S = \{(x,t) : x \in \{0, L\},\ t > 0\}$,
(iii) u satisfies (1.1) in the classical sense.
The local existence and uniqueness of such a solution is well known if the initial function u_0 belongs to $C([0, L])$ and if in addition it satisfies the compatibility conditions:

$$u_0(0) = 0 \qquad \text{and} \qquad u_0(L) = 0. \tag{3.1}$$

In Section 6 we establish bounds which enable us to extend this to global existence, and even uniform boundedness, for all $t \ge 0$.

It is clear from the definition given above that if $u(x,t)$ is a solution of Problem (1.1), then for any $t_0 > 0$ the function $u(\cdot, t_0)$ belongs to the Sobolev spaces $H_0^1(0, L)$ and $H^2(0, L)$.

We will frequently use the following calculus inequality that features the function

$$P(\xi) = (\xi^2 - 1)^2 - \alpha, \tag{3.2}$$

which was introduced in (1.14) in connection with the linear eigenvalue problem (1.12) associated with the Swift-Hohenberg equation (SH).

Lemma 3.1 *Let $L > 0$ be arbitrary. Then for any $u \in H_0^1(0, L) \cap H^2(0, L)$ we have*

$$\int_0^L \big\{(u'')^2 - 2(u')^2 + (1-\alpha)u^2\big\}\,dx \ge \mu \int_0^L u^2\,dx, \tag{3.3}$$

where

$$\mu = \inf\Big\{P\Big(\frac{n\pi}{L}\Big) : n \ge 1\Big\}. \tag{3.4}$$

Proof. Since $u \in H_0^1(0,L) \cap H^2(0,L)$ we can write u as a Fourier series in terms of the eigenfunctions φ_n (cf. (1.13)) of Problem (1.12):

$$u(x) = \sum_{n=1}^{\infty} a_n \varphi_n(x). \tag{3.5}$$

The left hand side of the inequality in (3.3) can then be written as

$$\frac{1}{L}\int_0^L \left\{(u'')^2 - 2(u')^2 + (1-\alpha)u^2\right\} dx = \sum_{n=1}^{\infty} P\Big(\frac{n\pi}{L}\Big)\, a_n^2. \tag{3.6}$$

Because the functions $P(\frac{n\pi}{L})$ are all bounded below by μ, and

$$\frac{1}{L}\int_0^L u^2\, dx = \sum_{n=1}^{\infty} a_n^2,$$

the assertion follows. $\square$

We conclude this section with a simple interpolation inequality that will prove useful later on.

Lemma 3.2 *Let $L > 0$ be arbitrary. Then for any $u \in H_0^1(0,L) \cap H^2(0,L)$ we have*

$$\int_0^L \left\{(u'')^2 - 2A(u')^2 + Bu^2\right\} dx \geq 0, \tag{3.7}$$

provided the constants A and B obey the relation $A^2 \leq B$.

The proof of Lemma 3.2 is similar to that of Lemma 3.1: we again write u in terms of a Fourier series. Then the resulting expression is nonnegative as long as $A^2 \leq B$. $\square$

4 The linear problem

Before turning to the full nonlinear problem we will establish various properties of the linear problem that results if we linearise the Swift-Hohenberg equation around the trivial solution $u = 0$:

$$\begin{cases} u_t = -u_{xxxx} - 2u_{xx} - (1-\alpha)u & \text{for} \quad (x,t) \in Q, \\ u = 0 \quad \text{and} \quad u_{xx} = 0 & \text{for} \quad (x,t) \in S, \\ u(x,0) = u_0(x) & \text{for} \quad x \in (0,L). \end{cases} \tag{4.1}$$

Here we assume that $u_0 \in C([0,L])$ and $u_0(x) = 0$ for $x = 0$ and $x = L$.

Remark. In the larger part of this article we in addition assume that u_0 is symmetric with respect to $x = \frac{1}{2}L$. This assumption is inspired by the symmetry of the initial function used in the numerical simulations. In this section we do not make this restriction in order to keep the analysis more general.

Since $u_0 \in L^2(0,L)$, we can write the solution $u(x,t)$ of Problem (4.1) as a Fourier series:

$$u(x,t) = \sum_{n=1}^{\infty} a_n \varphi_n(x) e^{-\lambda_n t}, \tag{4.2}$$

where φ_n and λ_n are, respectively, the eigenfunctions and eigenvalues of the corresponding eigenvalue problem (1.12). The coefficients a_n in (4.2) are given by $a_n = (u_0, \varphi_n)$. We recall that the eigenvalues are given by

$$\lambda_n = P\Big(\frac{n\pi}{L}\Big) \qquad \text{where} \qquad P(\xi) = (\xi^2 - 1)^2 - \alpha. \tag{4.3}$$

In Figure 3, the graphs of the functions $P(n\pi/L)$ are shown for $n = 1, 2, 3$. The expansion (4.2) implies that if $\lambda_n > 0$ for every $n \geq 1$, then the trivial solution $u = 0$ is linearly stable. On the other hand, if $\lambda_n < 0$ for at least one value of $n \geq 1$, then $u = 0$ is unstable. Therefore, we are interested in the sign of the eigenvalues λ_n.

Suppose that $\alpha \in (0,1)$. Under this assumption, the function $P(\xi)$ has two positive zeros, ξ_- and ξ_+ given by

$$\xi_- = \sqrt{1 - \sqrt{\alpha}} \quad \text{and} \quad \xi_+ = \sqrt{1 + \sqrt{\alpha}}. \tag{4.4}$$

Plainly, $P(\xi) < 0$ for $\xi_- < \xi < \xi_+$ and $P(\xi) > 0$ for $\xi < \xi_-$ and $\xi > \xi_+$. Note that as $\alpha \to 1^-$, then $\xi_-(\alpha) \to 0$, and ξ_- no longer exists when $\alpha > 1$. The zero ξ_+ exists for all $\alpha > 0$.

Related to the zeros of P we introduce the critical lengths:

$$L_1(\alpha) \stackrel{\text{def}}{=} \frac{\pi}{\xi_+} = \frac{\pi}{\sqrt{1 + \sqrt{\alpha}}} \quad \text{and} \quad L_2(\alpha) \stackrel{\text{def}}{=} \frac{\pi}{\xi_-} = \frac{\pi}{\sqrt{1 - \sqrt{\alpha}}}. \tag{4.5}$$

They are the zeros of the first eigenvalue $\lambda_1(\alpha)$, and $\lambda_1 < 0$ on (L_1, L_2). Plainly, the zeros of $\lambda_n(\alpha)$ are given by nL_1 and nL_2, and $\lambda_n < 0$ on (nL_1, nL_2). Note that L_1 is defined for all $\alpha > 0$ and L_2 for $\alpha \in (0,1)$.

We find that for L small enough, all the eigenvalues are positive. Specifically, if $L < L_1$, then

$$\frac{n\pi}{L} > \frac{n\pi}{L_1} \geq \frac{\pi}{L} = \xi_+ \qquad \text{for every} \quad n \geq 1,$$

and because $P(\xi)$ is increasing for $\xi \geq \xi_+$ this means that $\lambda_n = P(\frac{n\pi}{L}) > P(\xi_+) = 0$ for $n \geq 1$. Thus, when $L < L_1$, the trivial solution is linearly stable. We formulate this in the following theorem:

Theorem 4.1 *Let $u(x,t)$ be the solution of Problem (4.1), in which $\alpha > 0$. Suppose that*

$$L < L_1(\alpha). \tag{4.6}$$

Then

$$\|u(\cdot,t)\| \leq \|u_0\|\, e^{-\lambda_1 t} \qquad \textit{for} \quad 0 \leq t < \infty, \tag{4.7}$$

where $\|\cdot\|$ denotes the norm defined in (1.8), and

$$u(\cdot,t) \to 0 \qquad \textit{as} \qquad t \to \infty.$$

Proof. From (4.2) we deduce that

$$\|u(\cdot,t)\|^2 = \sum_{n=1}^{\infty} a_n^2 e^{-2\lambda_n t}, \tag{4.8}$$

where we have used the orthogonality and the normalisation of the eigenfunctions φ_n. For $L < L_1(\alpha)$, we have seen that $\lambda_n \ge \lambda_1$ for $n \ge 1$. Substituting this in (4.8) we find that

$$\|u(\cdot,t)\|^2 \le e^{-2\lambda_1 t} \sum_{n=1}^{\infty} a_n^2.$$

Since $\|u_0\|^2 = \sum_{n=1}^{\infty} a_n^2$ the assertion follows. □

Next, we focus on values of L that are larger than L_1. For such values of L one or several of the eigenvalues may become negative. It will be convenient to define the intervals

$$I_n = \Big\{ L > 0 : P\Big(\frac{n\pi}{L}\Big) \le 0 \Big\}, \qquad n \ge 1, \tag{4.9}$$

in which the eigenvalue λ_n is nonpositive; plainly $I_n = [nL_1, nL_2]$ for every $n \ge 1$.

For small values of α, the zeros L_1 and L_2 behave asymptotically as

$$L_1(\alpha) \sim \pi - \frac{\pi}{2}\sqrt{\alpha} \quad \text{and} \quad L_2(\alpha) \sim \pi + \frac{\pi}{2}\sqrt{\alpha} \quad \text{as} \quad \alpha \to 0^+. \tag{4.10}$$

Hence, the intervals I_n are centered around the points $n\pi$, and their lengths tend to zero as $\alpha \to 0$. Thus, for α and n small enough the intervals I_n will not overlap and are separated by intervals in which $\lambda_n > 0$. We refer to these intervals, where $\lambda_n \ge 0$ for all $n \ge 1$, as *Gaps*. Specifically, such a gap exists – between I_1 and I_2 – when

$$L_2 < 2L_1, \qquad \text{which holds for} \qquad 0 < \alpha < \alpha_1^* = \frac{9}{25} = 0.36.$$

Similarly, a second gap exists between I_2 and I_3 when

$$2L_2 < 3L_1 \qquad \text{i.e. if} \qquad 0 < \alpha < \alpha_2^* = \frac{25}{169} = 0.14792899.$$

Note that for this range of α-values there exist two gaps: one between I_1 and I_2 and one between I_2 and I_3. In general, let $n \ge 1$ be an arbitrary integer. Then there exists a gap between I_n and I_{n+1} when

$$0 < \alpha < \alpha_n^* = 4\Big((2n+1) + \frac{1}{2n+1}\Big)^{-2}. \tag{4.11}$$

The numbers α_n^* are seen to decrease with n. Therefore, if there is a gap between the intervals I_n and I_{n+1}, then there are gaps between I_m and I_{m+1} for every $m = 1, \dots, n$.

In Figure 3 we see that there is a gap between I_1 and I_2 but there are no gaps between the intervals I_n and I_{n+1} for $n \ge 2$.

The existence of these *Gaps*, when α is small enough, leads to an interesting new phenomenon, unknown in second order diffusion equations: asymptotic convergence to the trivial solution for values of L larger than L_1. As an example we consider the case when $\alpha < \alpha_1^*$, which implies that there is at least a gap between I_1 and I_2.

Theorem 4.2 *Suppose that* $0 < \alpha < \alpha_1^*$, *and*

$$L_2(\alpha) < L < 2L_1(\alpha).$$

Then the solution $u(x,t)$ *of the linear problem (4.1) converges to the trivial solution as* $t \to \infty$ *according to the rate*

$$\|u(\cdot,t)\| \leq \|u_0\|\, e^{-\mu(L)t} \qquad \textit{for} \quad 0 \leq t < \infty, \tag{4.12}$$

where $\mu(L) = \min\{\lambda_n(L) : n \geq 1\} = \min\{\lambda_1, \lambda_2\} > 0$.

A similar result can be established for values of L in the set

$$\mathcal{S}_n \stackrel{\text{def}}{=} (0, L_1) \cup (L_2, 2L_1) \cup (2L_2, 3L_1) \cup \cdots \cup (nL_2, (n+1)L_1) \qquad \text{for} \quad \alpha < \alpha_n^*.$$

This set $\mathcal{S}_n$ includes the first n gaps. We obtain:

Theorem 4.3 *Suppose that* $0 < \alpha < \alpha_n^*$, *and* $L \in \mathcal{S}_n$. *Then the solution* $u(x,t)$ *of the linear problem (4.1) converges to the trivial solution as* $t \to \infty$ *according to the rate*

$$\|u(\cdot,t)\| \leq \|u_0\|\, e^{-\mu(L)t} \qquad \textit{for} \quad 0 \leq t < \infty, \tag{4.13}$$

where $\mu(L) = \min\{\lambda_n(L) : n \geq 1\} > 0$.

The proof of this theorem is based on the same ideas as the proof of Theorem 4.1.

Next, we consider values of L for which at least one of the eigenvalues is negative. As L increases, it passes through the bounded sets I_n in whose interior the corresponding eigenvalues λ_n are negative. In this manner successive terms in the Fourier expansion of u_0, involving the eigenfunctions φ_n, will grow with time. The one for which $|\lambda_n|$ is largest will become dominant as time tends to infinity and so determines the large time behaviour. Thus, we define the sets

$$\omega_n = \{L \in I_n : \lambda_n < \lambda_k \;\; \text{for} \;\; k \geq 1, \;\; k \neq n\}. \tag{4.14}$$

The sets ω_1, ω_2 and ω_3 are shown in Figure 3.

We are now ready to state the relation between the length L of the domain and the profile of the solution that is selected as $t \to \infty$.

Theorem 4.4 *Let* $n \geq 1$. *If* $L \in \omega_n$ *and* $a_n \neq 0$, *then*

$$e^{\lambda_n t} u(x,t) \to a_n \varphi_n(x) \qquad \textit{as} \quad t \to \infty.$$

Proof. We write the Fourier series (4.2) of u as

$$e^{\lambda_n t} u(x,t) - a_n \varphi_n(x) = \sum_{k=1\ (k\neq n)}^{\infty} e^{(\lambda_n - \lambda_k)t} a_k \varphi_k(x). \tag{4.15}$$

Since $L \in \omega_n$, it follows that λ_n is the smallest eigenvalue, and that $\lambda_n - \lambda_k < 0$ for every $k \geq 1$ such that $k \neq n$. Hence, the right hand side in (4.15) decays exponentially to zero as $t \to \infty$.

Thus, as L increases and passes through the sets ω_n, the solution of Problem (4.1) *selects different dominant modes* φ_n as $t \to \infty$, resulting in different limiting patterns.

5 Local behaviour near $\mathbf{L_1}$ and $\mathbf{L_2}$

In the numerical studies described in Section 2 we have seen how in the (L, v)-plane, branches of nontrivial stationary solutions bifurcate from the trivial solution at $L = L_1$ and at $L = L_2$ (see Figures 2 and 9). In this section we study these bifurcations: we prove that unique smooth branches $u_1(L)$ and $u_2(L)$ bifurcate from $u = 0$ at, respectively, the lengths L_1 and L_2 defined in Section 4, and we derive expressions for the norm $\|u\|$, the action $J(u; L)$ and the energy $\mathcal{E}(u; L)$ along these branches in the neighbourhood of these bifurcation points.

It will be convenient to scale the spatial variable x to a fixed interval $[0, 1]$. Thus, we introduce the variables $\tilde{x}$ and $\tilde{u}$:

$$x = L\tilde{x} \qquad \text{and} \qquad u(x) = \tilde{u}(\tilde{x}). \tag{5.1}$$

To keep the notation simple, we shall henceforth omit the tildes again.

In terms of the new variables a stationary solution $u(x)$ of Problem (1.1) will be a solution of the following problem:

$$\begin{cases} \mathcal{L}(u; L) + L^4 u^3 = 0 & \text{for} \quad x \in (0, 1), \\ u = 0, \quad u'' = 0 & \text{at} \quad x = 0,\ 1, \end{cases} \tag{5.2}$$

where

$$\mathcal{L}(u; L) = u^{iv} + 2L^2 u'' + L^4(1 - \alpha)u. \tag{5.3}$$

The corresponding eigenvalue problem for the linear operator $\mathcal{L}$ is

$$\begin{cases} \mathcal{L}(u; L) = \sigma u & \text{for} \quad x \in (0, 1), \qquad \sigma = L^4\lambda, \\ u = 0, \quad u'' = 0 & \text{at} \quad x = 0,\ 1, \end{cases} \tag{5.4}$$

where λ is the eigenvalue of the corresponding problem prior to scaling. The eigenvalues σ_n are given by

$$\sigma_n = L^4\lambda_n = L^4 P\left(\frac{n\pi}{L}\right) = \{(n\pi)^2 - L^2\}^2 - L^4\alpha,$$

and the corresponding eigenfunctions ψ_n are

$$\psi_n(x) = \sqrt{2}\,\sin(n\pi x).$$

We first focus on the bifurcation at $L = L_1$, where L_1 is the unique root of the equation

$$(\pi^2 - L^2)^2 - L^4\alpha = 0$$

in the interval $(0, \pi)$; it is given in (4.5). Since we intend to study the relation between u and L near the point $(L, u) = (L_1, 0)$ we write

$$L = L_1(1 + \xi) \qquad \text{and} \qquad u = \varepsilon(\psi_1 + w), \tag{5.5}$$

where $\varepsilon > 0$ is a small constant, and ξ and w will turn out to be small quantities. Substitution into the full equation (5.2) yields the following equation for v:

$$\mathcal{L}(w; L_1) = h(w, \xi, \gamma), \qquad \gamma = \varepsilon^2, \tag{5.6}$$

where

$$\begin{aligned}h(w,\xi,\gamma) = &-2L_1^2\{(1+\xi)^2-1\}(\psi_1''+w'')\\&-L_1^4\{(1+\xi)^4-1\}(\psi_1+w)(1-\alpha)\\&-\gamma\,L_1^4(1+\xi)^4(\psi_1+w)^3.\end{aligned} \tag{5.7}$$

We now use Lin's method (cf. [16],[12]). We introduce the subspaces X_0 and X_1 of $X = L^2(\Omega)$ defined by

$$X_0 = \{s\psi_1 : s \in \mathbf{R}\} \quad \text{and} \quad X_1 = \{z \in X : (z,\psi_1) = 0\}, \tag{5.8}$$

and we denote the orthogonal projection of X onto X_0 by $\mathcal{P}$. We then first solve the problem

$$\begin{cases}\mathcal{L}(w;L_1) = (I-\mathcal{P})h(w,\xi,\gamma) & \text{for} \quad x \in (0,1),\\ w,\ w'' = 0 & \text{at} \quad x = 0,\ 1.\end{cases} \tag{5.9}$$

The right hand side in (5.9) is an element of X_1, and the operator $\mathcal{L}(\cdot;L_1)$ is nonsingular on X_1. By a standard contraction argument one can show that for some small constant $\rho > 0$ there exists a unique solution $w^*(\xi,\gamma)$ of Problem (5.9) as long as $|\xi| < \rho$, $|\gamma| < \rho$ and $\|w\| < \rho$, such that $w^*(0,0) = 0$. This solution will be a solution of the original equation (5.6) if

$$\mathcal{P}h(w^*(\xi,\gamma),\xi,\gamma) = 0,$$

which means that

$$\mathcal{G}(\xi,\gamma) \stackrel{\text{def}}{=} \int_0^1 \psi_1 h(v^*(\xi,\gamma),\xi,\gamma)\,dx = 0. \tag{5.10}$$

By standard ODE theory, w^* is a smooth function of ξ and γ, and hence $\mathcal{G}$ is also a smooth function of ξ and γ. Thus, by applying the Implicit Function Theorem, we find that if $\mathcal{G}_\xi(0,0) \neq 0$, then ξ is a differentiable function of γ, and

$$\mathcal{G}_\xi \frac{d\xi}{d\gamma} + \mathcal{G}_\gamma = 0 \qquad \text{and} \qquad \xi(0) = 0,$$

so that

$$\frac{d\xi}{d\gamma} = -\frac{\mathcal{G}_\gamma}{\mathcal{G}_\xi}, \tag{5.11}$$

where $\mathcal{G}_\xi$ and $\mathcal{G}_\gamma$ are computed at the origin.

An elementary calculation shows that

$$\begin{aligned}&h(0,0,0) = 0, && h_v(0,0,0) = 0,\\ &h_\xi(0,0,0) = -4L_1^2\psi_1'' - 4L_1^4(1-\alpha)\psi_1, && h_\gamma(0,0,0) = -L_1^4\psi_1^3.\end{aligned}$$

Thus,

$$G_\gamma(0,0) = -L_1^4\int_0^1 \psi_1^4\,dx = -\frac{3}{2}L_1^4,$$

and

$$\begin{aligned}G_\xi(0,0) &= -4L_1^2\int_0^1 \psi_1''\psi_1\,dx - 4L_1^4(1-\alpha)\int_0^1 \psi_1^2\,dx\\ &= 4\pi^2L_1^2 - 4L_1^4(1-\alpha) = 4\pi^2\sqrt{\alpha}L_1^2,\end{aligned}$$

where we have used the expression (4.5) for L_1. Therefore

$$\frac{d\xi}{d\gamma}(0,0) = \frac{3}{8\pi^2}\frac{L_1^2}{\sqrt{\alpha}} = \frac{3}{8}\frac{1}{\sqrt{\alpha}\,(1+\sqrt{\alpha})}, \tag{5.12}$$

from which we conclude that

$$\xi = \frac{3}{8}\gamma\frac{1}{\sqrt{\alpha}\,(1+\sqrt{\alpha})} + \text{h.o.t.}$$

Note also that

$$\int_0^1 u^2\,dx = \varepsilon^2\int_0^1 \psi_1^2\,dx + \text{h.o.t} = \varepsilon^2 + \text{h.o.t} = \gamma + \text{h.o.t},$$

and

$$\xi = \frac{L-L_1}{L_1}.$$

Therefore

$$\int_0^1 u^2\,dx \sim \gamma \sim \frac{8}{3\pi}\sqrt{\alpha}\,(1+\sqrt{\alpha})^{3/2}(L-L_1) \qquad \text{as} \quad L \searrow L_1. \tag{5.13}$$

Finally returning to the original variables, and using that

$$\|u\|^2 = \frac{1}{L}\int_0^L u^2\,dx = \int_0^1 \tilde{u}^2\,d\tilde{x},$$

we have proved the following theorem.

Theorem 5.1 *Let $\alpha > 0$. There exists a unique branch in the (L,u)-plane of nontrivial solutions of Problem (5.2) which emanates from the trivial solution at L_1, i.e. from the point $(L,u) = (L_1, 0)$. Its local behaviour is given by*

$$\|u\|^2 \sim \frac{8}{3\pi}\sqrt{\alpha}\,(1+\sqrt{\alpha})^{3/2}(L-L_1) \qquad \text{as} \quad L \searrow L_1.$$

In an entirely analogous manner we can prove the following theorem about the local behaviour near L_2 when $0 < \alpha < 1$. We omit the proof.

Theorem 5.2 *Let $0 < \alpha < 1$. There exists a unique branch in the (L,u)-plane of nontrivial solutions of Problem (5.2) which emanates from the trivial solution at L_2, i.e. from the point $(L,u) = (L_2, 0)$. Its local behaviour is given by*

$$\|u\|^2 \sim \frac{8}{3\pi}\sqrt{\alpha}\,(1-\sqrt{\alpha})^{3/2}(L_2-L) \qquad \text{as} \quad L \nearrow L_2.$$

Remark. For larger values of α we will have $3L_1 < L_2$, and solutions near L_2 will not have lowest action. Therefore, these solutions will unsually not feature as final states of Problem (1.1).

Arguing along the same lines we can derive expressions for $J(u;L)$ and $\mathcal{E}(u;L)$ when L is close to L_1 or to L_2 (and $0 < \alpha < 1$).

Theorem 5.3 *On the branch defined in Theorem 5.1 we have*

$$J(u;L) \sim -\frac{8}{3\pi^2}\alpha\,(1+\sqrt{\alpha})^3(L-L_1)^2 \qquad as \quad L \searrow L_1,$$

and

$$\mathcal{E}(u;L) \sim -\frac{16}{3\pi}\alpha(1+\sqrt{\alpha})^{5/2}(L-L_1) \qquad as \quad L \searrow L_1.$$

Theorem 5.4 *On the branch defined in Theorem 5.2 we have for* $0<\alpha<1$,

$$J(u;L) \sim -\frac{8}{3\pi^2}\alpha\,(1-\sqrt{\alpha})^3(L_2-L)^2 \qquad as \quad L \nearrow L_2,$$

and

$$\mathcal{E}(u;L) \sim \frac{16}{3\pi}\alpha(1-\sqrt{\alpha})^{5/2}(L_2-L) \qquad as \quad L \nearrow L_2.$$

Remark. We deduce from Theorems 5.3 and 5.4 that $\mathcal{E}(u;L)<0$ in a left-neighbourhood of L_1, and $\mathcal{E}(u;L)>0$ in a right-neighbourhood of L_2, Therefore, assuming that $\mathcal{E}(u;L)$ depends continuously on L in (L_1,L_2), there exists a length $L_0 \in (L_1,L_2)$ such that $\mathcal{E}(u;L_0)=0$.

6 Global bounds

In this section we establish a series of a-priori bounds for solutions of the full nonlinear problem (1.1). This results in the identification of balls in $L^2(0,L)$ and in $H_0^1(0,L)$ into which all orbits – regardless of their initial data – eventually enter. In particular, these results will show that the values of L for which solutions of the *linear* problem – discussed in Section 4 – tend to $u=0$, are *precisely* the values of L for which solutions of the full *nonlinear* problem also tend to the trivial solution. Some related bounds were recently given in [2] and [3].

For convenience we recall

$$\mu(L)=\min\{\lambda_n(L): n=1,2,\dots\}. \tag{3.4}$$

In this section we shall not assume that the initial value u_0 in Problem (1.1) is symmetric with respect to $x=\frac{1}{2}L$.

Let $u(t)=u(x,t)$ be the solution of Problem (1.1). We begin with a bound for the L^2-norm $\|u(t)\|$ defined in (1.8).

Theorem 6.1 *Let* $u(t)$ *be the solution of Problem (1.1), and let* μ *be defined in (3.4).*
(a) *Suppose that* $\mu>0$. *Then*

$$\|u(t)\| \le \|u_0\|e^{-\mu t} \qquad for \quad 0\le t<\infty, \tag{6.1}$$

and

$$u(t) \to 0 \qquad as \quad t \to \infty \quad in \quad L^2(0,L).$$

(b) *Suppose that* $\mu = 0$. *Then*

$$\|u(t)\| \le \frac{\|u_0\|}{\sqrt{1 + 2\|u_0\|^2\, t}} \qquad for \quad 0 \le t < \infty, \tag{6.2}$$

and

$$u(t) \to 0 \qquad as \quad t \to \infty \quad in \quad L^2(0,L).$$

(c) *Suppose that* $\mu < 0$. *Then*

$$\|u(t)\| \le \max\{\|u_0\|, \sqrt{|\mu|}\} \qquad for \quad 0 \le t < \infty, \tag{6.3}$$

and

$$\limsup_{t\to\infty} \|u(t)\| \le \sqrt{|\mu|}. \tag{6.4}$$

Proof. We multiply equation (1.1a) by u and integrate the resulting equation over the spatial domain $(0, L)$. After a few integrations by parts of the right hand side of the equation, in which the boundary conditions (1.1b) are used, we derive the identity

$$\frac{1}{2}\frac{d}{dt}\int_0^L u^2\,dx = -\int_0^L \big\{(u_{xx})^2 - 2(u_x)^2 + (1-\alpha)u^2\big\}\,dx - \int_0^L u^4\,dx.$$

Applying Lemma 3.1 to estimate the first integral on the right hand side, we obtain

$$\frac{1}{2}\frac{d}{dt}\int_0^L u^2\,dx \le -\mu\int_0^L u^2\,dx - \int_0^L u^4\,dx. \tag{6.5}$$

From Schwarz's inequality we deduce that

$$\int_0^L u^2\,dx \le \sqrt{L}\,\Big(\int_0^L u^4\,dx\Big)^{1/2},$$

so that

$$\|u\|^2 = \frac{1}{L}\int_0^L u^2\,dx \le \Big(\frac{1}{L}\int_0^L u^4\,dx\Big)^{1/2}. \tag{6.6}$$

Using this inequality to bound the last integral in (6.5), we obtain, after dividing by L, the differential inequality

$$Y_0' \le -2\mu Y_0 - 2Y_0^2, \qquad \text{where} \qquad Y_0 = Y_0(t) = \|u(t)\|^2, \tag{6.7}$$

in which the prime denotes differentiation with respect to t.

If $\mu > 0$, we readily deduce from (6.7), that

$$Y_0(t) \le Y_0(0)\, e^{-2\mu t} \qquad \text{for} \quad 0 \le t < \infty,$$

from which (6.1) follows. If $\mu = 0$, we find that

$$Y_0(t) \le \frac{Y_0(0)}{1 + 2Y_0(0)\,t} \qquad \text{for} \quad 0 \le t < \infty,$$

which implies (6.2).
Finally, if $\mu < 0$, we can only conclude, by looking at the flow of Y_0 and using the fact that $Y_0 > 0$, that

$$Y_0(t) \le \max\{Y_0(0), |\mu|\} \qquad \text{for} \quad 0 \le t < \infty,$$

which yields (6.3). Therefore,

$$\limsup_{t\to\infty} Y_0(t) \le |\mu|. \qquad \square$$

Summarising, if $\mu \ge 0$, then the origin is a global attractor in $L^2(0, L)$, and if $\mu < 0$ the global attractor is contained in the ball B_R in $L^2(0, L)$, with radius $R = \sqrt{|\mu|}$, and centered at the origin.

Bounds, like the ones given in Theorem 6.1 for $\|u\|$, can also be established for $\|u_x\|$:

Theorem 6.2 *Let $u(t)$ be the solution of Problem (1.1), and let μ be defined in (3.4). Then*

$$\begin{aligned} \|u_x(t)\| &= O(e^{-\mu t}) \quad &\textit{as} \quad t \to \infty \qquad &\textit{if} \quad \mu > 0, \\ \|u_x(t)\| &= O(t^{-1/2}) \quad &\textit{as} \quad t \to \infty \qquad &\textit{if} \quad \mu = 0, \end{aligned}$$

and

$$\limsup_{t\to\infty} \|u_x(t)\| \le \{2(1+\alpha)\}^{1/4}\sqrt{|\mu|} \qquad \textit{if} \quad \mu < 0.$$

Proof. We differentiate equation (1.1a) with respect to x, multiply by u_x and integrate over $(0, L)$. After some integrations by parts in which the boundary conditions are applied, we arrive at the identity

$$\begin{aligned} \frac{1}{2}\frac{d}{dt}\int_0^L (u_x)^2\,dx = &-\int_0^L \left\{(u_{xxx})^2 - 2(u_{xx})^2 + (1-\alpha)(u_x)^2\right\} dx \\ &- 3\int_0^L u^2 (u_x)^2\,dx. \end{aligned}$$

By omitting the second integral on the right, and rearranging the terms in the first integral, we obtain

$$\begin{aligned} \frac{1}{2}\frac{d}{dt}\int_0^L (u_x)^2\,dx \le &-\frac{1}{2}\int_0^L (u_{xxx})^2 - 4(u_{xx})^2 + 4(u_x)^2\big\}\,dx \\ &- \frac{1}{2}\int_0^L (u_{xxx})^2\,dx + (1+\alpha)\int_0^L (u_x)^2\,dx. \end{aligned}$$

We now use Lemma 3.2 applied to u_x, and put $A = 2$ and $B = 4$. This yields

$$\frac{1}{2}\frac{d}{dt}\int_0^L (u_x)^2\,dx \le -\frac{1}{2}\int_0^L (u_{xxx})^2\,dx + (1+\alpha)\int_0^L (u_x)^2\,dx. \tag{6.8}$$

In order to estimate the term involving u_{xxx} we use the following inequality.

Proposition 6.1 *Let $u \in H_0^1(0,L)$ be such that $u_{xx} \in H_0^1(0,L)$. Then*

$$\|u_x\|^3 \le \|u\|^2 \|u_{xxx}\|. \tag{6.9}$$

We postpone the proof of Proposition 6.1 to the end of this section and continue with the proof of Theorem 6.2.

Using (6.9) to eliminate the term involving u_{xxx} from (6.8) yields the differential inequality

$$Y_1' \le -\frac{Y_1^3}{Y_0^2} + 2(1+\alpha)Y_1, \qquad \text{where} \qquad Y_1 = \|u_x(t)\|^2. \tag{6.10}$$

We treat the cases $\mu > 0$, $\mu = 0$ and $\mu < 0$ in succession.

(1) $\underline{\mu > 0}$: Invoking Theorem 6.1, we find that

$$Y_1' \le -Ae^{4\mu t}Y_1^3 + 2(1+\alpha)Y_1, \qquad A = Y_0^{-2}(0).$$

By classical ODE theory this implies that

$$Y_1(t) \le Z(t),$$

where Z is the solution of the problem

$$Z' = -Ae^{4\mu t}Z^3 + 2(1+\alpha)Z, \qquad Z(0) = Y_1(0).$$

Writing

$$Z(t) = z(t)e^{-2\mu t},$$

we find that z satisfies the autonomous equation

$$z' = 2(1+\alpha+\mu)z - Az^3.$$

Regardless of the (positive) values of α, μ and A, and the initial value $z(0)$, the solution z is uniformly bounded, so that there exists a constant $K_1 > 0$ such that

$$Y_1(t) \le K_1 e^{-2\mu t} \qquad \text{for} \quad 0 \le t < \infty,$$

which yields the first estimate of Theorem 6.2.

(2) $\underline{\mu = 0}$: Proceeding as in Case (1), we now find that

$$Y_1' \le -\Big(\frac{1+2Bt}{B}\Big)^2 Y_1^3 + 2(1+\alpha)Y_1, \qquad B = Y_0(0).$$

To estimate $Y_1(t)$ we use the comparison function $Z(t) = z(t)(t+1)^{-1}$. An elementary computation shows that $z(t)$ is uniformly bounded and hence that there exists a constant $K_2 > 0$ such that

$$Y_1(t) \le K_2(t+1)^{-1} \qquad \text{for} \quad 0 \le t < \infty.$$

(3) $\underline{\mu < 0}$: We recall from Theorem 6.1 that

$$\limsup_{t\to\infty} Y_0(t) \le |\mu|.$$

When we use this upper bound for Y_0 in (6.10), the assertion readily follows. $\square$

Remark. Due to the Sobolev imbedding theorem [1], which states that if $u \in H_0^1(0,L)$, then $u \in L^\infty(0,L)$ and

$$\|u\|_\infty \le \sqrt{\frac{L}{2}}\,\|u_x\|,$$

Theorem 6.2 also yields a bound for u in $L^\infty(0,L)$.

Proof of Proposition 6.1. Integration by parts, and using the boundary conditions we obtain,

$$\int_0^L (u_x)^2\,dx = -\int_0^L u\,u_{xx}\,dx.$$

By Schwarz's inequality,

$$\Big|-\int_0^L u\,u_{xx}\,dx\Big| \le \Big(\int_0^L u^2\,dx\Big)^{1/2}\Big(\int_0^L (u_{xx})^2\,dx\Big)^{1/2}.$$

Using this in the first identity we conclude that

$$\int_0^L (u_x)^2\,dx \le \Big(\int_0^L u^2\,dx\Big)^{1/2}\Big(\int_0^L (u_{xx})^2\,dx\Big)^{1/2}. \tag{6.11}$$

In an analogous fashion we find that

$$\int_0^L (u_{xx})^2\,dx \le \Big(\int_0^L (u_x)^2\,dx\Big)^{1/2}\Big(\int_0^L (u_{xxx})^2\,dx\Big)^{1/2}. \tag{6.12}$$

Combining (6.11) and (6.12) yields the desired inequality. $\square$

7 Properties of the symmetric minimiser

In Section 2 we followed solutions of Problem (1.1) numerically in time, and we saw how they converge to a final state v as $t \to \infty$. These states are equilibrium states of Problem (1.1) and usually a minimiser – global or local – of the functional $J(u;L)$ defined in (1.4) when such states are isolated. The numerically obtained graphs of $J(v;L)$ are shown in Figures 4 and 10.

In this section we focus on the *global minimiser* u of the variational problem

$$\Phi(L) = \min\{J(w,L) : w \in H^2(0,L)\cap H_0^1(0,L),\ w(x) = w(L-x)\}. \tag{7.1}$$

Note that by construction u will be symmetric. We establish bounds for $\Phi(L)$ as well as for $\|u\|$, and we show that $J(u;L) = \mathcal{E}(u;L)$ at those values of L where $\Phi(L)$ has a local minimum. In addition, we analyse the *Shape* of the global minimiser. We do this for values of L in the set ω_1 defined in (4.14). This implies that *(i)* $\lambda_1(L) < 0$, and *(ii)* $\lambda_1(L)$ is the smallest eigenvalue. In view of the symmetry of the minimiser, we only need to take into account the eigenvalues λ_n for which n is odd. Therefore

$$\omega_1 = \{L \in (L_1, L_2) : \lambda_1(L) < \lambda_3(L)\}.$$

We will be concerned here with the branch of symmetric solutions that bifurcates from the trivial solution at L_1, and in our analysis we assume that these solutions are global minimisers. In Section 5 we have seen that the branch bifurcating at L_1 is unique. Hence when L is close to L_1 this uniqueness implies that these solutions are global minimisers. We conjecture that this is the case for all $L \in \omega_1$.

We begin with an upper bound for $J(u; L)$.

Theorem 7.1 *Let u be a global minimiser of Problem (7.1). Then*

$$J(u; L) \le -\frac{1}{6}\left|P\left(\frac{\pi}{L}\right)\right|^2 \qquad \text{for} \quad L_1 < L < L_2. \tag{7.2}$$

Proof. The proof is based upon the selection of a suitable test function. We put

$$w(x) = a\varphi_1(x),$$

where a is a constant that will be chosen later and φ_1 is the eigenfunction that corresponds to the first eigenvalue λ_1. Because u is a global minimiser, J takes on its smallest value when we substitute u. Therefore,

$$J(u) \le J(a\varphi_1) = \frac{1}{2}a^2 P\left(\frac{\pi}{L}\right) + \frac{3}{8}a^4.$$

Since $P(\frac{\pi}{L}) < 0$ for $L_1 < L < L_2$ we can write this as

$$J(u) \le J(a\varphi_1) = -\frac{1}{2}a^2\left|P\left(\frac{\pi}{L}\right)\right| + \frac{3}{8}a^4. \tag{7.3}$$

We can still choose a, and we do this in such a way that the right hand side of (7.3) is minimal. This is the case when

$$a^2 = a_0^2 \stackrel{\text{def}}{=} \frac{2}{3}\left|P\left(\frac{\pi}{L}\right)\right|. \tag{7.4}$$

Substituting this value for a into (7.3) yields the upper bound stated above. □

Next, we obtain a lower bound for $J(u; L)$.

Theorem 7.2 *Let u be a global minimiser of Problem (7.1). Then*

$$J(u; L) \ge -\frac{1}{4}\left|P\left(\frac{\pi}{L}\right)\right|^2 \qquad \text{for} \quad L \in \omega_1. \tag{7.5}$$

Proof. For $L \in \omega_1$, Lemma 3.1 gives that

$$J(u; L) \ge -\frac{1}{2}\left|P\left(\frac{\pi}{L}\right)\right|\|u\|^2 + \frac{1}{4L}\int_0^L u^4\,dx.$$

The integral can be estimated using (6.6) so that we obtain

$$J(u;L) \geq -\frac{1}{2}\Big|P\Big(\frac{\pi}{L}\Big)\Big|\|u\|^2 + \frac{1}{4}\|u\|^4 \geq -\frac{1}{4}\Big|P\Big(\frac{\pi}{L}\Big)\Big|^2,$$

where the last inequality was obtained by minimising the resulting polynomial in $\|u\|^2$. $\square$

Remark. Making a Taylor expansion of $P(\frac{\pi}{L})$ around L_1, and using the explicit expression (4.5) for L_1 shows that

$$\Big|P\Big(\frac{\pi}{L}\Big)\Big| \sim \frac{4}{\pi}\sqrt{\alpha}(1+\sqrt{\alpha})^{3/2}(L-L_1) \qquad \text{as} \quad L \searrow L_1. \tag{7.6}$$

When we apply Theorem 5.3 to estimate J near L_1, and use (7.6), we find that

$$\lim_{L\to L_1} \frac{J(u;L)}{|P(\frac{\pi}{L})|^2} = -\frac{1}{6}. \tag{7.7}$$

This shows that the upper bound obtained in Theorem 7.1 is asymptotically sharp in the limit as $L \to L_1$.

Graphs of the upper and lower bound for J obtained in Theorems 7.1 and 7.2 are shown in Figure 14, together with the graph of J for the final profile v. Near the bifurcation points L_1 and $3L_1$ the graph of $J(v;L)$ dips slightly below the lower bound because of numerical error.

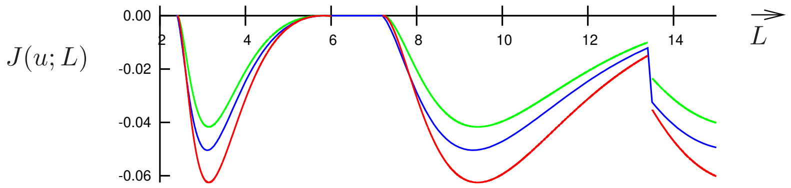

Figure 14: Upper and lower bound for the action $J(u;L)$ (blue) of the numerically obtained final profile v when $\alpha = 0.3$.

For $\|u\|$ we find the following bounds:

Theorem 7.3 *Let u be a global minimiser of Problem (7.1). Then*

$$\Big(1-\frac{1}{\sqrt{3}}\Big)\Big|P\Big(\frac{\pi}{L}\Big)\Big| \leq \|u\|^2 \leq \Big(1+\frac{1}{\sqrt{3}}\Big)\Big|P\Big(\frac{\pi}{L}\Big)\Big| \qquad \textit{for} \quad L \in \omega_1. \tag{7.8}$$

Proof. Combining Theorem 7.1 and the second inequality in the proof of Theorem 7.2, we conclude that

$$-\frac{1}{6}\Big|P\Big(\frac{\pi}{L}\Big)\Big|^2 \geq J(u;L) \geq -\frac{1}{2}\Big|P\Big(\frac{\pi}{L}\Big)\Big|\|u\|^2 + \frac{1}{4}\|u\|^4,$$

which gives

$$\|u\|^4 - 2\,\Big|P\Big(\frac{\pi}{L}\Big)\Big|\|u\|^2 + \frac{2}{3}\Big|P\Big(\frac{\pi}{L}\Big)\Big|^2 \leq 0.$$

The left hand side is a quadratic polynomial in $\|u\|^2$, which can only take on nonnegative values in the range of $\|u\|^2$ as given in (7.8). $\square$

In the numerical simulations we found that $J = \mathcal{E}$ at local minima of J. For periodic minimisers of J on the real line, this equality is well known (see [11], [17] and [19]). In the next theorem we formulate this observation precisely, and prove its validity.

Theorem 7.4 *Let for some $\delta > 0$,*

$$\Phi_\delta(\overline{L}) = \min\{\Phi(L) : L \in (\overline{L}(1-\delta), \overline{L}(1+\delta)\},$$

and let $\overline{w}$ be a minimiser so that $\Phi_\delta(\overline{L}) = J(\overline{w}, \overline{L})$. Then

$$J(\overline{w}, \overline{L}) = \mathcal{E}(\overline{w}, \overline{L}).$$

Proof. By appropriately scaling the minimiser $\overline{w}(x)$, we define the family of functions

$$w_\lambda(x) = \overline{w}(\lambda x) \qquad \text{for} \quad \lambda \in (\lambda_-, \lambda_+),$$

where $\lambda_\pm = 1/(1 \mp \delta)$. We intruduce the function

$$H(\lambda) \stackrel{\text{def}}{=} J\Big(w_\lambda, \frac{\overline{L}}{\lambda}\Big).$$

Plainly,

$$H(1) = J(\overline{w}, \overline{L}) = \Phi_\delta(\overline{L}) \qquad \text{and} \qquad H(\lambda) \ge \Phi(\overline{L}/\lambda) \ge \Phi_\delta(\overline{L}) \quad \text{for} \quad \lambda \in (\lambda_-, \lambda_+).$$

Therefore, $H(\lambda)$ has a minimum at $\lambda = 1$. Since H is a smooth function, this means that $H'(1) = 0$.

We find that

$$\begin{aligned} H(\lambda) &= \frac{\lambda}{L} \int_0^{L/\lambda} \Big\{ \frac{1}{2}\big(w_\lambda''(x)\big)^2 - \big(w_\lambda'(x)\big)^2 + F_\alpha\big(w_\lambda(x)\big) \Big\}\, dx, \\ &= \frac{1}{L} \int_0^{L} \Big\{ \frac{1}{2}\lambda^4\big(w''(y)\big)^2 - \lambda^2\big(w'(y)\big)^2 + F_\alpha\big(w(y)\big) \Big\}\, dy, \end{aligned}$$

where we have omitted the overbars, and put $y = \lambda x$. Thus,

$$H'(\lambda) = \frac{1}{L} \int_0^L \Big\{ 2\lambda^3\big(w''(y)\big)^2 - 2\lambda\big(w'(y)\big)^2 \Big\}\, dy.$$

Since $H'(1) = 0$, we conclude that

$$\int_0^L \Big\{ 2\big(w''(y)\big)^2 - 2\big(w'(y)\big)^2 \Big\}\, dy = 0.$$

We divide this expression by L and subtract the result from $H(1)$ to obtain

$$\begin{aligned} \Phi(L) &= \frac{1}{L} \int_0^L \Big\{ -\frac{3}{2}\big(w''(x)\big)^2 + \big(w'(x)\big)^2 + F_\alpha\big(w(x)\big) \Big\}\, dx, \\ &= \frac{1}{L} \int_0^L \Big\{ w'(x)w'''(x) - \frac{1}{2}\big(w''(x)\big)^2 + \big(w'(x)\big)^2 + F_\alpha\big(w(x)\big) \Big\}\, dx. \end{aligned}$$

The integrand in the last integral is nothing but the energy functional $\mathcal{E}(\overline{w};\overline{L})$, where we have put the overbars back again. Since it is constant along orbits, we have shown that

$$\Phi(\overline{L}) = J(\overline{w};\overline{L}) = \mathcal{E}(\overline{w},\overline{L}). \qquad \square$$

We now turn to a study of the shape of the global minimiser u for that part of the interval ω_1 in which $\lambda_3(L) > 0$, i.e. the interval $\omega_1 \cap (L_1, 3L_1)$.

For L near L_1 the solution looks like a small multiple of the first eigenfunction φ_1 at L_1. In the numerical simulations shown in Section 2 (see Figures 6b, 7a and 8a), it was noted that, even when L is not close to L_1, the solutions still look like a (no longer small) multiple of the first eigenfunction φ_1 corresponding to L. Here we give an explanation of this observation, and we show that it is intimately connected to the fact that the differential operator in Problem (1.1) is of fourth order.

To make the above observation about the shape of u more precise, we write

$$u = a_1\varphi_1 + w, \qquad a_1 = (u, \varphi_1). \tag{7.9}$$

Therefore, we have chosen w in such a way that it lies in the orthogonal complement of the ray $\mathcal{S} = \{s\varphi_1 : s \in \mathbf{R}\}$. We want to estimate the size of w relative to that of the component $a_1\varphi_1$ of u in $\mathcal{S}$. Since $\|\varphi_1\| = 1$, this means that we need to estimate the quantity

$$\tan\theta \stackrel{\text{def}}{=} \frac{\|w\|}{a_1}, \tag{7.10}$$

where θ is the angle between u and $\mathcal{S}$. We obtain the following result.

Theorem 7.5 *Let u be a symmetric global minimiser of Problem (7.1), and let θ be the angle between u and the ray $\mathcal{S}$ spanned by φ_1. Then*

$$\tan^2\theta = \frac{\|w\|^2}{a_1^2} \le \frac{1}{4}\sqrt{3}\,(\sqrt{3}+1)\,\frac{\left|P\left(\frac{\pi}{L}\right)\right|}{P\left(\frac{3\pi}{L}\right)} \qquad \textit{for} \quad L \in \omega_1 \cap (L_1, 3L_1). \tag{7.11}$$

Proof. We split $J(u;L)$ into a quadratic and a higher order part:

$$J(u;L) = J_1(u;L) + J_2(u;L),$$

where

$$J_1(u;L) = \frac{1}{L}\int_0^L \left\{\frac{1}{2}(u'')^2 - (u')^2 + \frac{1-\alpha}{2}u^2\right\} dx,$$

and

$$J_2(u;L) = \frac{1}{4L}\int_0^L u^4\,dx.$$

Because u is symmetric and so is φ_1, it follows that w is symmetric. This implies that the Fourier expansion of w contains no term involving φ_2 and starts with a term involving φ_{2k+1}

where $k \geq 1$. Applying an argument similar to that used in the proof of Lemma 3.1, we obtain the inequality

$$J_1(w) \geq \frac{1}{2} P\Big(\frac{3\pi}{L}\Big) \|w\|^2 \qquad \text{if} \quad L < 3L_1.$$

Since w and φ_1 are orthogonal, and J_2 is positive, this yields the following lower bound:

$$\begin{aligned} J(u) = J(a_1\varphi_1 + w) &= J_1(a_1\varphi_1) + J_1(w) + J_2(a_1\varphi_1 + w) \\ &\geq a_1^2 J_1(\varphi_1) + \frac{1}{2} P\Big(\frac{3\pi}{L}\Big) \|w\|^2. \end{aligned} \tag{7.12}$$

On the other hand, since u is a global minimiser,

$$J(u) \leq J(a_1\varphi_1) = a_1^2 J_1(\varphi_1) + a_1^4 J_2(\varphi_1). \tag{7.13}$$

Upon combining (7.12) and (7.13) we find that

$$\|w\|^2 \leq \frac{2\, J_2(\varphi_1)\, a_1^4}{P\big(\frac{3\pi}{L}\big)} = \frac{3\, a_1^4}{4P\big(\frac{3\pi}{L}\big)},$$

and hence

$$\frac{\|w\|^2}{a_1^2} \leq \frac{3}{4P\big(\frac{3\pi}{L}\big)}\, a_1^2. \tag{7.14}$$

It remains to estimate a_1^2. Invoking the orthogonality of w and φ_1 once more, we deduce that

$$\|u\|^2 = a_1^2 + \|w\|^2 \geq a_1^2.$$

We then use Theorem 7.3 to bound $\|u\|$ from above to derive an upper bound for a_1^2:

$$a_1^2 \leq \|u\|^2 \leq \Big(1 + \frac{1}{\sqrt{3}}\Big) \Big| P\Big(\frac{\pi}{L}\Big) \Big|. \tag{7.15}$$

Substituting (7.15) into (7.14) we arrive at the upper bound stated in Theorem 7.4. $\square$

Example. Let $L_0 = \pi$ and $\alpha = 0.3$. Then it is readily seen that $L_0 \in \omega_1 \cap (L_1, 3L_1)$. An explicit calculation shows that

$$P\Big(\frac{3\pi}{L_0}\Big) = P(3) = (9-1)^2 - 0.3 = 63.7.$$

Using this in the bound for $\tan\theta$ in Theorem 7.4 we find that

$$\tan^2\theta = \frac{\|w\|^2}{a_1^2} \leq 0.0055715,$$

which is indeed a very small number. Thus, for $L = \pi$, which is close to where $J(u; L)$, as a function of L, attains its minimum value, and $\alpha = 0.3$, the global minimiser is still very close to a suitable multiple of $\varphi_1(x) = \sqrt{2}\sin(\frac{\pi x}{L})$.

Inspection of the right hand side of (7.11) shows that an important reason for θ being so small is that the function $P(\frac{n\pi}{L})$ is a *fourth order* polynomial in n, which, even for $n = 3$ – as in the denominator of (7.11) – is already quite large. It is clear that for, say, sixth order equations, the polynomial $P(\frac{n\pi}{L})$ will be of sixth order in n, causing θ to be still smaller [8].

References

[1] Adams, R.A., *Sobolev spaces*, Academic Press, New York, 1975.

[2] Bartucelli, M.V. *On the positivity of solutions of the extended Fisher-Kolmogorov equetion with nonlinear diffusion*, Math. Methods Appl. Sc. **25** (2002) 701-708.

[3] Bartucelli, M.V., S.A. Gourley & A.A. Ilyin, *Positivity and attractivity in a fourth-order reaction-diffusion equation*, Proc. Roy. Soc. London, Series A **458** (2002) 1431-1446.

[4] Berg, J.B. van den & R.C.A.M. van der Vorst, *Stable patterns for fourth order parabolic equations*, to appear in Duke Math. J. (2002).

[5] Bodenschatz, E., W. Pesch & G. Ahlers, *Recent developments in Rayleigh-Bénard convection*, Ann. Rev. Fluid Mech. **32** (2000) 709-778.

[6] Berg, G.J.B. van den, L.A. Peletier & W.C. Troy, *Global branches of multiu-bump periodic solutions of the Swifth-Hohenberg equation*, Arch. Rational Mech. Anal. **158** (2001) 91-153.

[7] Chaparova, J., *Existence and numerical approximation of periodic solutions of semilinear fourth order differential equations*, J. Math. Anal. Appl. (2003) in press.

[8] Chaparova, J., L.A. Peletier & S. Tersian, *Existence and nonexistence of nontrivial solutions of semilinear sixth order ordinary differential equations*, to appear in Appl. Math. Letters, 2003.

[9] Collet, P. & J.P. Eckmann, *Instabilities and fronts in extended systems*, Princeton Series in Physics, Princeton University Press, 1990.

[10] Cross, M.C. & P.C. Hohenberg, *Pattern formation outside of equilibrium*, Rev. Mod. Phys. **65** (1993) 851-1112.

[11] Dananivć, V. & A. Bjeliš, *General criteria for stability of uniaxially ordered states if incommensurate-commensurate systems*, Phys. Rev. Lett. **80** (1998) 10-13.

[12] Hale, J.K., L.A. Peletier & W.C. Troy. *Exact homoclinic and heteroclinic solutions of the Gray-Scott model for autocatalysis*, SIAM. J. Appl. Math. **61** (2000) 102-130.

[13] Hale, J.K., *Asymptotic behavior of dissipative systems*, Mathematical Surveys and Monographs #25, American Mathematical Society, Providence RI, 1988.

[14] Hohenberg, P.C. & J.B. Swift, *Effects of additive noise at the onset of Rayleigh-Bénard convection*, Phys. Rev. A **46** (1992) 4773.

[15] Lega, J., J.V. Moloney & A.C. Newell, *Swift-Hohenberg equation for lasers*, Phys. Rev. Lett. **73** (1994) 2978-2981.

[16] Lin, X.-B., *Using Mel'nikov's method to solve Sil'nikov's problems*, Proc. Royal Soc. Edinburgh, **116A** (1990) 295-325.

[17] Pomeau, Y., & P. Manneville, *Wave length selection in cellular flows*, Phys. Letters **75A** (1980) 296-298.

[18] Peletier, L.A. & V. Rottschäfer, *Large time behaviour of solutions of the Swift-Hohenberg equation*, C. R. Acad. Sci. Paris, Ser I. **336** (2003) 225-230.

[19] Peletier, L.A. & W.C. Troy, *Spatial patterns: Higher order models in physics and mechanics*, Birkhäuser, Boston, 2001.

[20] Peletier, L.A., W.C. Troy & R.C.A.M. van der Vorst, *Stationary solutions of a fourth order nonlinear diffusion equation*, Differential'nye Uravneniya **31** (1995) 327-337 (in Russian) Differential Equations **31** (1995) 301-314 (in English).

[21] Swift, J.B., & P.C. Hohenberg, *Hydrodynamic fluctuations at the convective instability*, Phys. Rev. A **15** (1977), 319–328.

[22] Tersian, S., & J. Chaparova, *Periodic and homoclinic solutions of the extended Fisher-Kolmogorov equation*, J. Math. Anal. Appl. **260** (2001) 490-506.